




Universitetet
i Stavanger

FACULTY OF SCIENCE AND TECHNOLOGY

MASTER'S THESIS

Study programme/specialisation: M.Sc. in Environmental Engineering	Spring / Autumn semester, 2017. Open/ Confidential
Author: Konstantinos Pappas Zountouridis	 (signature of author)
Programme coordinator: Roald Kommedal Supervisor(s): Torleiv Bilstad, Knut Erik Teigen Giljarhus, Bjørn Erling Vembe	
Title of master's thesis: Large Eddy Simulation of buoyant plumes	
Credits: 30	
Keywords: Environmental risk CFD LES Turbulence model Buoyant plume CCS safety	Number of pages:92..... + supplemental material/other: Stavanger, ...15.06.2017..... date/year

Large Eddy Simulation of buoyant plumes

Konstantinos Pappas Zountouridis

June 2017

MASTER THESIS PROJECT



Universitetet
i Stavanger

M.Sc. in Environmental Engineering
Department of Mathematics and Natural Sciences
University of Stavanger, Norway

Preface

In this Master thesis project, turbulence models for fluid flows are investigated to simulate thermal, helium and CO₂ dispersion, in order to tackle challenges in environmental risk and safety engineering. The work was carried out throughout the spring semester of 2017 for the completion of the M.Sc programme in Environmental Engineering, at the University of Stavanger. The university's supervisor is professor Torleiv Bilstad, while external supervisors are Knut Erik Teigen Giljarhus from Lloyd's Register Consulting - Energy AS and Bjørn Erling Vembe from Computational Industry Technologies AS.

Stavanger, Norway , 15.06.2017

Konstantinos Pappas Zountouridis

Acknowledgements

I am grateful for the help and support I got from Knut Erik Teigen Giljarhus from Lloyd's Register Consulting - Energy AS and Bjørn Erling Vembe from Computational Industry Technologies AS (ComputIT AS). Their professional expertise has had an influence on the quality of this project.

There are several people that have to be mentioned for their role in the process. Starting chronologically, special thanks to my friend Dimitrios Kostopoulos from Total E&P Norge, who introduced me to Bjørn Erling Vembe and the idea of the project was created, together with the fundamental additions by Knut Erik Teigen Giljarhus. Many thanks to Torleiv Bilstad and Evgenia Protasova from the University of Stavanger for their immediate help when requested. A word of mention also for the people of ComputIT AS, for their hospitality coupled with their technical support during my stay in Trondheim.

Thanks also to my friends:

- Matteo Busi, Ph.D. candidate at the Technical University of Denmark, for providing the Latex template that this report is based on along with tutorials
- Konstantinos Dimitrakopoulos, M.Sc. candidate at Uppsala University, for his help in tackling challenges encountered in the software packages
- Bianca Handley from the US Environmental Protection Agency, for thoroughly checking the report and making edifying comments
- Alexandros Kordalis, M.Sc. candidate at the National Technical University of Athens, for his tips in writing Python scripts
- Aris Xylouris from Analysys Mason, for improving the structure and the expressions in this report with his linguistic advices.

Finally but most importantly, I would like to thank my family, Ioannis, Theopisti, and Elisavet, that gave me the possibility and encouragement to study abroad.

K.P.Z.

Abstract

Industrial and environmental safety relies on understanding and evaluating risks and failures on the individual processes and operations. Simulating hazardous fluid flows with the use of Computational Fluid Dynamics (CFD) software is an accepted technique to assess consequences, and construct protective barriers in case of a negative event.

Some well-documented flow scenarios with significant properties that need to be further investigated are the buoyancy-dominated plumes, and the multiphase flow from a high pressure liquid CO₂ release. The model that will mimic the turbulence in the system is one of the numerous parameters to be considered when conducting a fluid flow simulation.

This project focuses on evaluating Large Eddy Simulation (LES) turbulence models in the buoyant plumes. The models depend on different filtering techniques for the eddy resolution (temporal and spatial), and the goal is to recognize the main factors and challenges affecting such simulations, by comparing numerical to experimental data.

Three different test cases are simulated, one thermal plume, one helium plume, and one CO₂ release. In the thermal plume case, the numerical and the experimental data are closely matching, while for the helium plume the models overpredict the experimental data. The numerical data for CO₂ give insights into a high pressure release from a pipeline rupture, which can be encountered in Carbon Capture and Storage (CCS) infrastructures. Apart from the choice of the turbulence model, imposing random fluctuations in the inlet of the flow, the grid scale of the setup and the writing interval of the time-averaged data are distinguished as key features with large impact on the simulation efforts.

Keywords: Environmental risk, CFD, LES, turbulence model, buoyant plume, CCS safety

Nomenclature

Hellenic Characters

Δ	filter width, grid width
δ_{ij}	Kronecker delta
ϵ	kinetic energy dissipation term
η	Kolmogorov length scale
κ	wavenumber
μ	viscosity
ϕ	molecular stress term
ρ	density
τ	simulation time
τ_{ij}	Reynolds stress term

Latin Characters

c_e	coefficient of the dissipation term
C_k	Kolmogorov constant
c_p	specific heat
c_t	coefficient of the stress term

D	diameter
E	energy spectrum
g	gravitational constant
H, h	enthalpy
k	thermal conductivity
L	length scale
l	length scale
N	number of grid nodes
P, p	pressure
p^1	hydrodynamic pressure
Q	heat flux
R	gas constant
R_{ij}	Reynolds stress term
Re	Reynolds number
S_{ij}	molecular strain rate tensor
T	temperature
t	time
t_{ij}	stress term
U	internal energy
u	velocity
V	volume

Superscripts

\hat{X} filtered variable with arbitrary filter

\bar{X} filtered variable with arbitrary filter

\tilde{X} Favre-filtered variable with arbitrary filter

Abbreviations

CCS Carbon Capture and Storage

CFD Computational Fluid Dynamics

CPU Central Processing Unit

DNS Direct Numerical Simulation

DOEEV Dynamic One-Equation Eddy-Viscosity

EOR Enhanced Oil Recovery

IDLH Immediately Dangerous to Life and Health Value

KFX Kameleon FireEx

LES Large Eddy Simulation

NIOSH US National Institute for Occupational Safety and Health

OpenFOAM Open-source Field Operation And Manipulation

RANS Reynolds-Averaged Navier-Stokes

RMS Root Mean Square

SGS Sub-Grid Scale

TFNS Temporally-Filtered Navier-Stokes

List of Figures

- 2.1 Predicted (KFX) and measured (Exp) maximum mole fractions of CO₂ (%) versus downstream distance for the BP test (Rian et al., 2014). 11
- 2.2 Predicted (KFX) and measured (Exp) maximum mole fractions of CO₂ (%) versus downstream distance for the Shell test (Rian et al., 2014). 11
- 2.3 Predicted and measured concentrations of CO₂ (% v/v) versus axial distance for the INERIS 2 tests with Phast, ANSYS-CFX, and FLACS (Gant et al., 2014). 12
- 2.4 Predicted and measured concentrations of CO₂ (% v/v) versus axial distance for the INERIS 8 tests with Phast, ANSYS-CFX, and FLACS (Gant et al., 2014). 13

- 3.1 Resolution levels of DNS, LES, RANS methods (figure adapted from CFD lecture material at Dartmouth College, USA (2006)). 22
- 3.2 Comparison of the simulation detail levels between DNS, LES, RANS methods (figure from CFD course material at the University of Stavanger, Norway (2017)). 22
- 3.3 Three dimensional flow topologies (figure adapted from De Villiers (2006)). 24

- 4.1 Illustration of the domain (Kumar and Dewan, 2014). 30
- 4.2 Snapshot of the initial conditions on the ground surface. 32
- 4.3 KFX doozer interface. 35
- 4.4 Development of the plume after 30 seconds simulation time in KFX, with an iso-surface value of 0.3. 37

4.5	Snapshots of the axial velocity magnitude taken at 30 seconds simulation time on a slice of the domain at the center of the geometry in OpenFOAM, for the coarse (L) and the medium (R) grid. The variation of the detail between the grids is visible.	38
4.6	Snapshot of the axial velocity magnitude taken at 30 seconds simulation time on a slice of the domain at the center of the geometry in KFX.	38
4.7	Centerline averaged axial velocity against the distance from the source for the thermal plume ($\tau = 30$ s).	39
4.8	Centerline averaged temperature against the distance from the source for the thermal plume ($\tau = 30$ s).	40
4.9	Turbulent kinetic energy spectrum for the thermal plume in OpenFOAM ($\tau = 30$ s).	41
5.1	Structure of the helium experiment (figure adapted from Chung and Devaud (2008), relating to the setup of Tieszen (2005)).	43
5.2	Representation of the domain across z direction. Cells are horizontally rectangular near the walls, and become denser and vertically rectangular closer to the centerline.	45
5.3	Geometry of the helium case in KFX from an external view (L) and without the chimney (R).	47
5.4	Development of the helium plume at 20 seconds with iso-surface value of 0.5. The puffing effect described in the start of this chapter is present.	49
5.5	Snapshot of the axial velocity magnitude taken on a slice of the domain at the center of the geometry in OpenFOAM, at 20 seconds simulation time.	50
5.6	Snapshot of the axial velocity magnitude taken on a slice of the domain at the center of the geometry in KFX, at 20 seconds simulation time.	51
5.7	Centerline averaged axial velocity against the distance from the source for the helium plume ($\tau = 20$ s).	52

6.1	COSHER experiment structure (figure from Total E&P Norge presentation by Pacaud, F and Tonda, H during KFX user meeting in Trondheim, Norway (2014).)	54
6.2	Aerial view of the COSHER experiment during 300 seconds after the release (figure adapted from Total E&P Norge presentation by Pacaud, F and Tonda, H during KFX user meeting in Trondheim, Norway (2014).)	55
6.3	Surface presentation of the CO ₂ concentrations 30 seconds after the release, along the wind direction.	58
6.4	CO ₂ concentrations downstream of the crater towards the wind direction at 30 seconds, for gentle and fresh wind conditions.	59
6.5	CO ₂ concentrations from 50 meters downstream of the crater towards the wind direction at 30 seconds, for gentle and fresh wind conditions.	60
7.1	OpenFOAM results for the helium case, for fluctuation scales in the inlet of value 0.5, 1, 2 and 4.	62
7.2	Centerline axial velocity results between the coarse and the fine grid for the thermal plume in OpenFOAM, $\tau = 30$ s.	64
7.3	Temperature results between the coarse and the fine grid for the thermal plume in OpenFOAM, $\tau = 30$ s.	65
7.4	KFX results for the helium plume, with a data writing interval of 0.25 and of 1 second.	67
7.5	Centerline averaged axial velocity (L) and temperature (R) data for the thermal plume, without the insertion of random fluctuations in the inlet in OpenFOAM ($\tau = 30$ s)(indicative sketching).	68

List of Tables

- 2.1 Possible compositions of CO₂ streams after being captured by the three different technologies (Pham and Rusli, 2016). 7
- 4.1 Characteristics of the thermal plume simulations. 31
- 5.1 Characteristics of the helium plume simulations. 44
- 6.1 Characteristics of the CO₂ plume simulation. 56

Contents

Preface	i
Acknowledgements	ii
Abstract	iii
Nomenclature	iv
List of Figures	vii
List of Tables	x
1 Introduction	1
1.1 Background	1
1.2 Problem description	2
1.3 Collaboration with companies	2
1.4 CFD software	3
1.5 Objective	3
1.6 Outline of the report	4
2 High pressure liquid CO₂ releases	5
2.1 Detaining CO ₂	5
2.1.1 CO ₂ thermodynamics	7
2.2 CFD software overview	8
2.2.1 KFX®	8
2.2.2 DNV Phast®	8
2.2.3 ANSYS-CFX®	9
2.2.4 FLACS®	9

2.3	Testing and validation	10
3	Governing Flow Characteristics	14
3.1	Fundamental equations	14
3.1.1	Navier-Stokes equations	15
3.1.2	Mach number	16
3.1.3	Averaging Navier-Stokes	16
3.2	Turbulence	17
3.2.1	Direct Numerical Simulation	18
3.2.2	Reynolds-Averaged Navier Stokes	19
3.2.3	Large Eddy Simulation	20
3.2.4	Effects of turbulence	21
3.3	Adaptation to current study	25
3.3.1	LES model in OpenFOAM®	26
3.3.2	LES model in KFX®	27
4	Thermal Plume	29
4.1	Computational setup	30
4.2	Simulation with OpenFOAM®	31
4.2.1	OpenFOAM solver	32
4.2.2	Turbulence model	33
4.2.3	Boundary conditions	33
4.3	Simulation with KFX®	34
4.3.1	Parameter setup	34
4.4	Results	36
5	Helium Plume	42
5.1	Computational Setup	43
5.2	Simulation with OpenFOAM®	45
5.2.1	OpenFOAM solver	45
5.2.2	Turbulence model	45

5.2.3	Boundary conditions	46
5.3	Simulation with KFX®	46
5.3.1	Parameter setup	46
5.4	Results	48
6	CO₂ Plume	53
6.1	Computational Setup	53
6.2	Simulation with KFX®	57
6.2.1	Parameter setup	57
6.3	Results	57
7	Discussion	61
7.1	Fluctuations in the inlet	61
7.2	Grid scales	63
7.3	Data writing intervals	66
7.4	LES model	67
7.5	General remarks	69
8	Conclusions	71
8.1	Summing up	72
8.2	Recommendations for future work	73
	Bibliography	74

Chapter 1

Introduction

1.1 Background

This Master thesis project investigates simulation models for experimental cases of key interest in safety engineering. To understand the importance of this mission, the macroscopical view of the problem is initially introduced before the microscopical scale follows.

As technology has advanced, the complexity of individual processes in industrial activities has increased, increasing the difficulty to successfully manage, control and monitor risks associated with these activities. For human and environmental safety, it is of utmost importance to be able to make precise estimations of the underlying risks, in order to minimize the degree of uncertainty.

This is part of the greater risk analysis and management process, where the decision makers must utilize all tools they have in their toolbox to reach a final decision on the safety compliance of an activity. All risks involved are carefully considered, and by withstanding an unavoidable but hopefully minimized degree of uncertainty the decision is reached.

In the safety sector, it is widely accepted that Computational Fluid Dynamics (CFD) are a reliable and dependable tool which demonstrates the outcomes and effects of a possible failure in the operations. In particular, fire and explosion engineering is continuously refining CFD to produce more realistic and accurate simulations which can enhance protective planning, barrier system construction, and operations and maintenance management.

1.2 Problem description

The main problem is located in defining and modelling the behaviour of fluids in hazardous scenarios. Particularly for gases, the challenge is to develop realistic models for their dispersion in the ambient atmosphere after a leak or release. As most flows are well into the turbulent scale, simplifying techniques are necessary in order to reduce the computational cost of turbulence in the simulations. These turbulence models are optimized in CFD simulations in order to improve the estimate of the location of impacted areas, ambient concentrations, and to better determine the actions to be taken if such an event occurs.

However, there are many parameters to be considered with the development of a CFD simulation. The most usual debatable point is the balancing of accuracy and computational cost. A simulation is feasible only if the result is close enough to the actual realistic phenomenon, but also only if it can be produced with the available computational resources. In order to find the precise balance, the relevant literature must be considered and to some extent trial and error is an essential procedure. The choice of the turbulence model that will be used usually has an impact on the precision levels and on the computational cost of the simulation.

1.3 Collaboration with companies

For the development of this project, the fundamental structure of the test cases and the programming scripts are provided by Knut Erik Teigen Giljarhus from Lloyd's Register Consulting - Energy AS along with his valuable guidance. Bjørn Erling Vembe from Computational Industry Technologies AS grants access to one of the CFD softwares, and provides simulation data for the helium plume case and significant programming help.

The work conducted affects cases of interest in safety engineering, delivers results that are applicable in technical consultancy, and demonstrates the capabilities of the software that are utilized together with further validation of them. Beyond industrial interest, the topics studied have scientific roots and the main goal is to connect the recent progress in the studies of the phenomena to simulation models used in present-day applications.

1.4 CFD software

Two different software packages are utilized for the simulations included in this study.

- **OpenFOAM®**, ("Open source Field Operation And Manipulation") is a C++ toolbox for the development of numerical solvers for the solution of CFD problems. It is applicable among diverse areas of engineering and science, for both commercial and academic organisations. Since 2004, it has been released and developed by OpenCFD Ltd (OpenFOAM, 2017).
- **KFX®**, ("Kameleon FireEx") is a general purpose CFD code with a wide operational domain, used in research and development activities on turbulent flow and combustion. It is developed by Computational Industry Technologies AS (ComputIT), in cooperation with NTNU and SINTEF in Norway (Rian et al., 2014).

To conduct the CFD simulations for this project, the Cluster of the University of Stavanger was utilized, which contains two servers (gorina1, gorina2) with 80 and 24 shared CPU cores, respectively. The KFX simulations were conducted in a remote server which is set up by Computational Industry Technologies AS.

1.5 Objective

The main objective of this project is to validate the ability of certain turbulence models in OpenFOAM and KFX in simulating phenomena of key interest in safety engineering. The objective is divided into the following tasks:

1. Evaluating the turbulence model of each software in the test cases.
2. Setting up simulation parameters that provide accurate results.
3. Comparing the numerical results from the two software to experimental data.
4. Identifying the challenges faced in the simulation processes.

1.6 Outline of the report

Within the frames of the project, three different cases are studied: the thermal, helium and CO₂ plumes. After presenting the computational setups and validating the results for the first two, the more complex simulation of a CO₂ release is investigated.

The structure of the rest of this report begins with Chapter 2, where a study on the utilization of CFD software for Carbon Capture and Storage (CCS) facilities is included. The software capable of modelling high pressure liquid CO₂ releases from pipeline ruptures in such facilities are presented, along with the testing and validation that has already been conducted.

In Chapter 3, the fundamental laws of fluid flow and turbulence are introduced, in order to understand the theory in which the CFD software is based on. The adaptation of the governing flow equations to this study is presented, and the theory behind the turbulence model utilized in each software is defined.

Following up, Chapters 4,5 and 6 contain the simulation details and the results for the thermal, helium, and CO₂ plumes. These characteristics include solvers, turbulence models, domain and grid sizes used, time steps, and total simulation times. Numerical results are compared to the experimental data available for each case. For the thermal plume, measurements of axial velocity and temperature are available in the literature, whereas for the helium plume velocity measurements are available. There are no data for the CO₂ plume publicly available, but the concentrations of CO₂ along the release directions are estimated, to give an insight into the consequences of an actual release incident.

Discussion follows in Chapter 7, where the key elements that affect the simulations are pointed out and the challenges faced in the process are highlighted. Conclusions are summed up in Chapter 8, where recommendations for further work in the field are also delivered.

Chapter 2

High pressure liquid CO₂ releases

In this chapter, the background theory on high pressure liquid CO₂ releases is presented, along with the recent CFD validation that has been conducted. The aim is to demonstrate the relevance of simulating CO₂ releases to industrial applications, and highlight the challenges faced in previous efforts.

2.1 Detaining CO₂

Present day activities such as firing of fossil fuel have led to increased CO₂ generation into the atmosphere. It is believed that the implementation of Carbon Capture and Storage (CCS) technologies is a feasible way to tackle carbon emissions, and has also applications in Enhanced Oil Recovery (EOR) projects. However, CCS facilities entail the risk of hazardous release of CO₂ through potential ruptures in the pipeline and in the infrastructures.

There are three basic processes that take part in a CCS system:

1. Capturing CO₂ from large emission sources.
2. Compressing and transporting the captured CO₂.
3. Injection and storage of the CO₂ underground.

In these systems, pipelines have the important role of transporting high-pressurized liquid CO₂ from the capturing elements to the underground storage facilities (Pham and Rusli,

2016). Effective risk management of potential ruptures in these areas is of utmost importance. At standard conditions, CO₂ is a colorless, odorless gas undetectable by human senses. The US National Institute for Occupational Safety and Health (NIOSH) has set the Immediately Dangerous to Life and Health Value (IDLH) for CO₂ to 4% (Rian et al., 2014).

In order to design and successfully manage the risk involved in CCS infrastructures, better understanding is required about the consequences of dense phase CO₂ released into the atmosphere. In a high pressure release, it is transformed into a mixture of gaseous and solid CO₂ (dry ice) at ambient temperature and pressure (Gant et al., 2014). CO₂ will replace air near the ground as it is more heavy, so the asphyxiation hazard and toxic effects can be intense. The release conditions from the pipeline, where it is unleashed through an orifice into the atmospheric conditions without previous heat exchange with the environment, are described from the Joule-Thomson effect. The drop in pressure from the atmospheric conditions is accompanied by significant cooling. In thermodynamics, the Joule-Thomson process describes the temperature change of a real fluid when it is forced through a valve or a porous plug. The enthalpy, H , is considered constant, where:

$$H = U + PV \quad (2.1)$$

Therefore, with the PV product increasing, the internal energy, U , will decrease. This will result in very low ambient temperatures that are potentially harmful in the near field.

For the coming CCS projects, new pipelines will be built to transport CO₂ of varying components of impurities depending on the capturing technology used (post-combustion capture, oxyfuel capture and pre-combustion capture)(Pham and Rusli, 2016). The CO₂ streams will have different composition depending on the capture technology. Substances like hydrogen sulfide (H₂S), carbon monoxide (CO) and various hydrocarbons are likely to be present in the stream, as it is shown in Table 2.1. Many of them are far more dangerous than CO₂, as H₂S that has an IDLH value of 0.01% (Rian et al., 2014).

There are many challenges to be dealt with when a dispersion model is used to predict the behavior and the range of the toxic CO₂ cloud. The unusual conditions of the release present many difficulties in the realistic description of such an event. However, in recent

Table 2.1: Possible compositions of CO₂ streams after being captured by the three different technologies (Pham and Rusli, 2016).

Table 1 – Composition of CO ₂ stream for three capture technologies.						
Component	Oxyfuel		Post-combustion		Pre-combustion	
	CFPP	GFPP	CFPP	GFPP	CFPP	GFPP
	Concentration (vol%)					
H ₂ S	0	0	0	0	0.01–0.6	<0.01
CO	0	0	0	0	0.03–0.4	0.04
SO ₂	0.5	<0.01	<0.01	<0.01	0	0
NO	0.01	<0.01	<0.01	<0.01	0	0
CH ₄ +	0	0	0	0	0.01	2.0
H ₂	0	0	0	0	0.8–2.0	1
Ar/N ₂ /O ₂	3.7	4.1	0.01	0.01	0.03–0.6	1.3

CFPP = coal fired power plant; GFPP = gas fired power plant.

years, many models have been developed with quite representative simulations.

2.1.1 CO₂ thermodynamics

For the development and validation of computer dispersion models, field experiments have been conducted to investigate the dispersion of CO₂ release and collect the relevant data. To better capture real world conditions, parameters such as air temperature, humidity, wind velocity and obstacles have to be considered.

Carbon dioxide has a triple point at 5.18 bara and 216.59 K, and its critical point is at 73.8 bara and 304.13 K. In atmospheric conditions, pure CO₂ may exist in the gas phase, in the solid phase, or as a mixture of these. Gas phase is the stable state of carbon dioxide, and solid CO₂ will eventually sublime in such conditions. Before transport and storage, CO₂ is compressed into liquid or supercritical state. Therefore, an accidental release may result in a complex high-momentum multiphase flow including formation of solid CO₂ particles that disperse, sublime and potential deposition of these downstream the release point (Rian et al., 2014).

2.2 CFD software overview

2.2.1 KFX®

The main interest is to simulate the overall dispersion of the CO₂ cloud rather than the details of the complex flow structure of the underexpanded jet at the release point. A pseudo-source model is deployed to calculate equivalent expanded flow parameters to be used as inlet conditions.

The multiphase CO₂ dispersion is simulated using an Euler-Lagrange model, with the use of the pseudo-source model for establishment of the necessary input parameters during the release. The gas phase flow behavior is modelled by the Reynolds-Averaged Navier-Stokes (RANS) partial differential equations for conservation of mass, momentum, and energy for time-dependent three-dimensional turbulent flow in a gravitational field. Turbulence is modelled using the k- ϵ model (described later in Chapter 3) with standard constants and extended to cover the buoyancy effects (Rian et al., 2014).

For each numerical parcel of droplets/particles that represents a class of physical ones, eight differential equations are solved:

- three for the position (trajectory)
- three for the velocity (momentum)
- one for droplet mass, and one for droplet temperature (energy).

There are also evaporation and sublimation models for droplets and particles, and the flow interactions between the gas and solid phase are taken into account.

2.2.2 DNV Phast®

DNV Software produced Phast, a hazard-assessment tool to simulate the atmospheric release of flammable or toxic chemicals, including discharge and dispersion. The discharge model based on conservation of mass, momentum and energy is used for the expansion from the orifice to ambient pressure. The central characteristic of Phast is the Unified Dispersion Model (UDM), where sub-models for two-phase jets, different dispersions, pool

spreading/evaporation are incorporated. For the dispersing jet of CO₂, it is assumed that there is a homogeneous equilibrium in the two-phase flow. This is documented to be a valid approximation for free-jet releases of dense-phase CO₂, but through orifices with up to 50.8 mm diameter (Gant et al., 2014).

2.2.3 ANSYS-CFX®

ANSYS-CFX software is a general purpose CFD program that can be used to model dispersions of heavy gases. The dispersion model for two-phase CO₂ uses a Lagrangian particle-tracking model for simulation of sublimating solid CO₂ particles in the jet. To account for the drag between the CO₂ particles and the surrounding gas phase, the Schiller and Naumann drag model is combined with the Eddy Interaction Model.

The discrete particle is assumed to interact with a succession of eddies, where they are characterized by a certain velocity, time and length scales. When the interaction happens, the fluid fluctuating velocity is kept constant and the discrete particle is moved with respect to its equation of motion. After that, a new fluctuating velocity is sampled and the process gets repeated.

The effects of ambient humidity need to also be accounted for, and for that the modelled gas phase consisted of a mixture of three components :dry air, CO₂ gas and water vapour. Each of these phases is treated as an ideal gas. The water vapour condensation and evaporation processes are modelled by source terms in the continuity and energy equations (Gant et al., 2014).

In the source conditions for the CO₂ jet, entrainment boundaries with no imposed wind speed are used. It has been documented that dense-phase CO₂ jet dispersion behaviour is insensitive to the imposed wind conditions, due to the dominance of the jet momentum, for concentrations down to 1% v/v (Gant and Kelsey, 2012).

2.2.4 FLACS®

GexCon AS have developed FLACS, a CFD tool especially for consequence modelling. The two-phase CO₂ dispersion model also use a Lagrangian method for the solid CO₂ parti-

cles. FLACS uses conservation equations for mass, energy, and momentum; it solves RANS equations based on the k - ϵ turbulence model (Schleder and Martins, 2016). Moreover, the interaction between particles and turbulence is accounted for by source terms in the turbulent kinetic energy and dissipation rate equations (Gant et al., 2014).

Buoyancy and drag forces are considered, while the instantaneous fluid velocity seen by the particle, which is an unknown parameter in the particle momentum equation, is modelled through stochastic differential equations. Particle deposition and interaction with obstacles can be modelled, but particle-particle interactions such as collisions, breakup and coalescence are not taken into account (Woolley et al., 2014). FLACS has been validated against experimental data sets from the evaluation database for LNG vapor dispersion (Hansen et al., 2010), which has quite similar characteristics with CO₂.

2.3 Testing and validation

Diverse tests have been conducted in order to collect real data and successfully evaluate and validate the simulation models. Validation simulations for the CO₂ dispersion by the KFX software have been performed for both BP (Figure 2.1) and Shell (Figure 2.2) tests. In these simulations, CO₂ was stored in a liquid state and was released into the atmosphere, to result in the multiphase dispersion of gas and solid particles. Temperature and wind parameters were monitored. There is a satisfactory overall agreement between the predicted and the measured maximum mole fractions of CO₂, as it can be deduced from Figures 2.1, 2.2. The application of the pseudo-source model for release is beneficial for practical engineering dispersion simulations of high-pressure releases, with the drawback of inaccuracies in the near field predictions. The deviation in the measurements is also a result of the strong anisotropic turbulence effects for the gas cloud flow along the ground, which are ignored by the k - ϵ turbulence model (Rian et al., 2014).

Field-scale experiments were conducted by INERIS, as part of the EU-funded CO₂PipeHaz project. In these experiments, CO₂ was discharged into the atmosphere through orifices of different diameters and the different dispersion models were compared. For this study, the integral dispersion model DNV Phast and the two CFD models ANSYS-CFX and FLACS

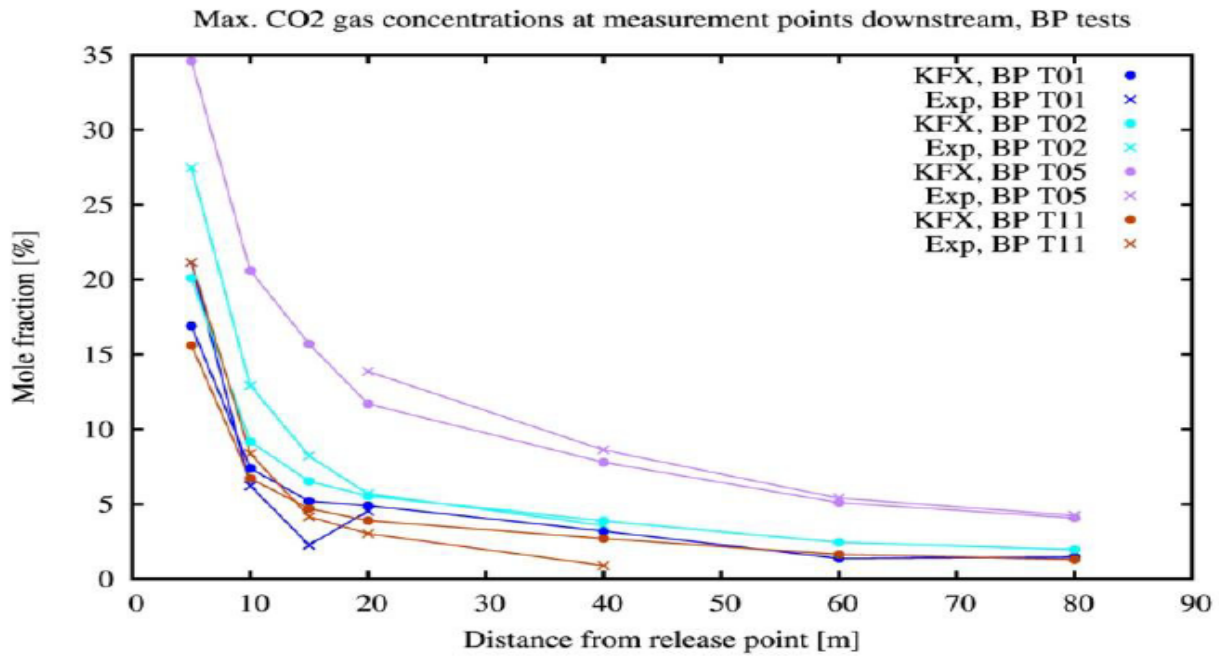


Figure 2.1: Predicted (KFX) and measured (Exp) maximum mole fractions of CO₂ (%) versus downstream distance for the BP test (Rian et al., 2014).

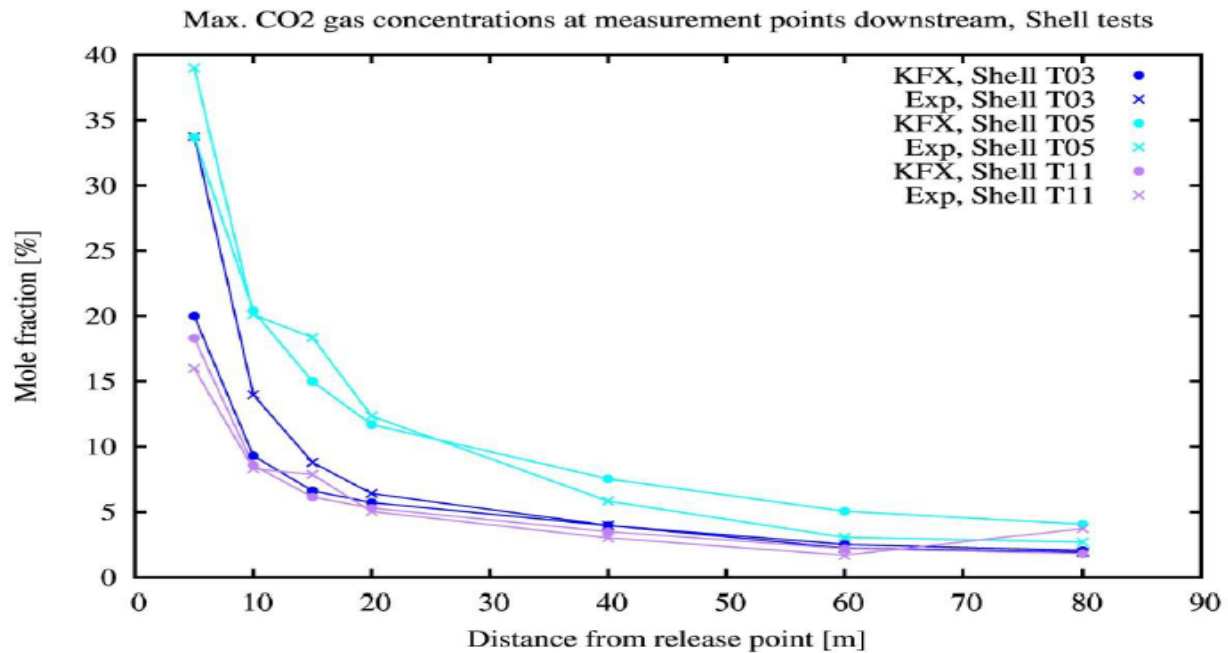


Figure 2.2: Predicted (KFX) and measured (Exp) maximum mole fractions of CO₂ (%) versus downstream distance for the Shell test (Rian et al., 2014).

were tested.

In the INERIS test 2 (Figure 2.3), all models predicted higher concentrations of CO₂ close to orifice (1m to 4m). Phast values were within 1% v/v of the ANSYS-CFX ones, and these were around 3-5% v/v higher than the measured values. FLACS predicted concentrations of 2% v/v higher than Phast and ANSYS-CFX. These differences can be quite significant, as it is mentioned before that the IDLH value of CO₂ is set to 4% v/v. In the INERIS test 8 (Figure 2.4), there is a disparity of around 8% v/v between the maximum and minimum prediction (twice the IDLH). Best results for ANSYS-CFX were available when the inlet boundary conditions were set from a model from the University of Leeds, where the axisymmetric, compressible RANS were solved and a degree of phase slip was allowed. Overall, there is reasonable agreement between the predicted and the measured concentrations, but there is high sensitivity in the models. The ANSYS-CFX model is sensitive to the way in which the inlet conditions are set, while FLACS is sensitive to the particle size of solid CO₂. (Gant et al., 2014).

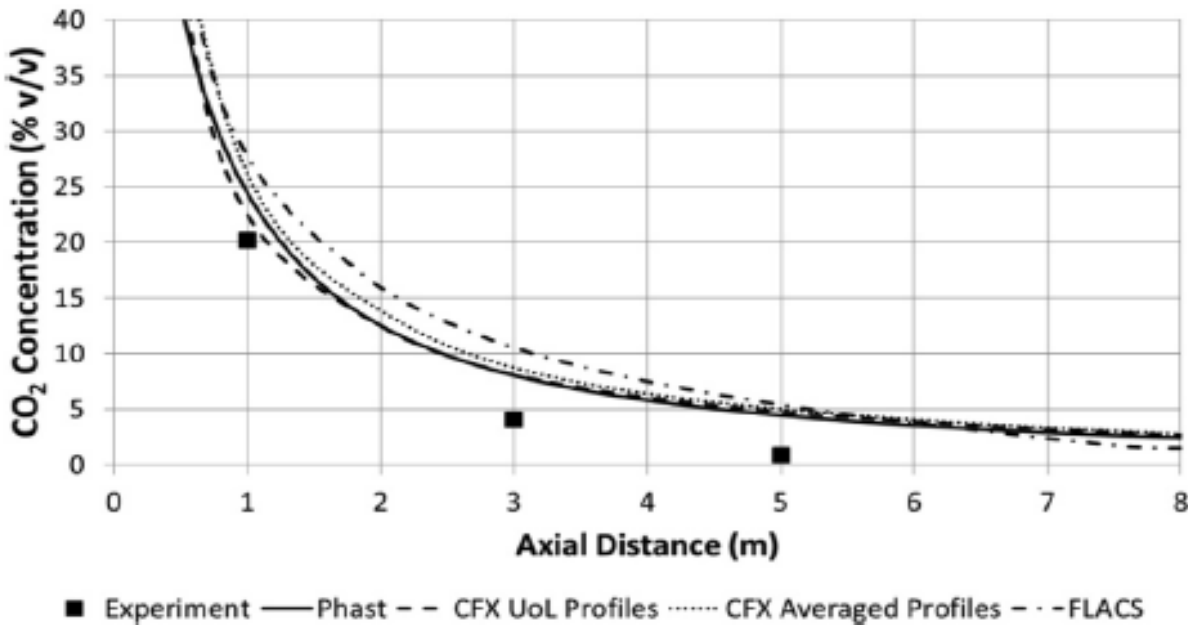


Figure 2.3: Predicted and measured concentrations of CO₂ (% v/v) versus axial distance for the INERIS 2 tests with Phast, ANSYS-CFX, and FLACS (Gant et al., 2014).

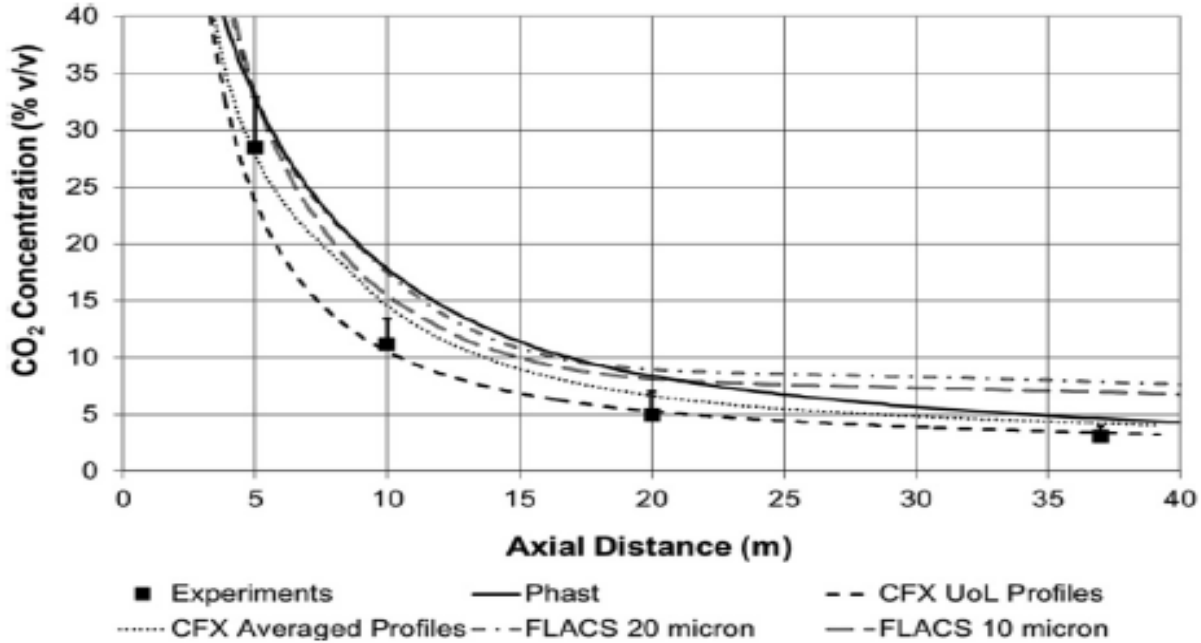


Figure 2.4: Predicted and measured concentrations of CO₂ (% v/v) versus axial distance for the INERIS 8 tests with Phast, ANSYS-CFX, and FLACS (Gant et al., 2014).

Studies must expand to cover dispersion scenarios when obstacles are present. Obstacles have important effects in how turbulence inside the CO₂ cloud is occurring, so they affect the simulations overall. The results of the CFD performance reproducing cloud dispersion in scenarios with obstacles need to be evaluated.

The wind is another parameter that needs to be dealt with in the simulations. In most of these, a constant wind is considered which is never the case in real data; Oscillations in wind speed and direction are always present. In a trial conducted by Schleder and Martins (2016) using FLACS, precision was lost when concentrations at a location out of the dispersion path axis were simulated. Deviations were documented between the predicted and measured concentrations at different positions, and that is highly likely because of the constant wind assumption that the model uses. There can be improvements in the performance of the simulations when more complex wind dynamics are considered. It has been observed that the modelling often agrees well with the experimental data in locations far from the center of the cloud (Fiates et al., 2016).

Chapter 3

Governing Flow Characteristics

The purpose of this chapter is to demonstrate the basic equations that govern flows in fluid dynamics. The concept of turbulence is introduced along with the models developed and the formation of equations that describe them.

3.1 Fundamental equations

To predict the behavior of physical systems, the existing models include some necessary simplifications in the form of idealised abstractions. The most basic assumption is the conservation of the following three important parameters that characterize fluid flow:

- Mass
- Momentum
- Energy

As it is well stated in the Master thesis of Lindroth (2013), the continuum hypothesis is assumed to hold; the molecular interactions in the fluid extend to a large enough scale that the fluctuations in the physical properties even out sufficiently, in order to be described by continuous fields. After this, the formulation of a set of equations modelling change in internal energy and motion of the fluid is possible. Further assumptions about the nature of the fluid include the concept of a fluid being incompressible, where pressure variations have no significant effect on density.

3.1.1 Navier-Stokes equations

Such assumptions led to the composition of the incompressible Navier-Stokes equations, and they were historically the first to be developed. However, in agreement with Worthy (2003), it makes more sense to derive the weakly compressible equations of this study by reducing the fully compressible ones. The dimensional compressible Navier-Stokes equations provided in Versteeg (2007) govern an ideal single component fluid for all speeds. However, the fact that all single component fluid equations are some sort of reduction of these, places them at the starting point when describing fluid flow.

$$\frac{\partial \rho}{\partial t} + \frac{\partial \rho u_i}{\partial x_i} = 0 \quad (3.1)$$

$$\frac{\partial \rho u_i}{\partial t} + \frac{\partial \rho u_i u_j}{\partial x_j} = -\frac{\partial P}{\partial x_i} + \frac{\partial \phi_{ij}}{\partial x_j} + \rho g_i \quad (3.2)$$

$$\frac{\partial U}{\partial t} + \frac{\partial u_j U}{\partial x_j} = \frac{k}{\rho} \frac{\partial^2 T}{\partial x_j^2} - \frac{P}{\rho} \frac{\partial u_i}{\partial x_j} + 2\nu(e_{ij}e_{ij} - \frac{1}{3}e_{ii}e_{jj}) \quad (3.3)$$

$$P = \rho RT \quad (3.4)$$

$$\phi_{ij} = 2\mu e_{ij} - \frac{2}{3}\delta_{ij}\mu e_{kk} \quad (3.5)$$

$$e_{ij} = \frac{1}{2}\left(\frac{\partial u_i}{\partial x_j} + \frac{\partial u_j}{\partial x_i}\right) \quad (3.6)$$

In these equations Einstein's convention of summation over repeated indices is adopted. For the indices that range over a given set of ($i = 1, 2, 3$):

$$y = \sum_{n=1}^3 x_n c^n = x_1 c^1 + x_2 c^2 + x_3 c^3$$

can be simplified to

$$y = x_i c^i$$

The first three equations comprise the continuity (3.1), the momentum (3.2) and the internal energy equation (3.3) respectively. Then the equation of state (3.4) is presented, while equation (3.5) represents the Stokes Hypothesis where the two coefficients of viscosity are linked. This implies that the thermodynamic pressure coincides with the mechanical pressure and characterizes the isotropic part of the complete stress tensor (3.6) (Buresti, 2015). The negative value between the parameters illustrates that if the fluid is locally expanding, there is a reduced tension requirement when a rate of stretching is applied along an axis. The parameter δ_{ij} in (3.5) is the Kronecker delta, for which:

$$\delta_{ij} = \begin{cases} 0, & \text{if } i \neq j, \\ 1, & \text{if } i = j. \end{cases}$$

3.1.2 Mach number

The Mach number is a dimensionless quantity that represents the ratio of the flow velocity to the speed of sound in the fluid ($M = \frac{u}{c}$). The gap between compressible and incompressible flows is bridged for lower Mach numbers, usually flows are treated as incompressible for values of $M = 0.3$ and smaller. In the present study, the flows have a low Mach number and that modifies the equations accordingly, a low-Mach-number weakly compressible formulation is used. This formulation includes density as an explicit variable in the computations (Zhou et al., 2001).

3.1.3 Averaging Navier-Stokes

In most engineering applications, the instantaneous equations are impossible to be solved directly, so some sort of averaging procedure needs to be undertaken. Otherwise, these equations have chaotic turbulent solutions, because of the high Reynolds numbers that are present in real applications. There are two different ways to average any dependent variable, Φ .

Reynolds averaging

In Reynolds averaging, the variable is averaged with respect to time. The variable Φ is decomposed into a fluctuating part Φ' and an average part $\bar{\Phi}$.

$$\bar{\Phi} \equiv \frac{1}{T} \int_T \Phi(t) \partial t$$

$$\Phi \equiv \Phi' + \bar{\Phi}$$

The parameter T is a time value long enough for the fluctuations in Φ to be resolved. This procedure is highly accurate in incompressible flows.

Favre averaging

For the Favre averaging, the decomposition of the variable Φ results into a fluctuating part Φ'' and a mean part $\tilde{\Phi}$ using a density weighted time average.

$$\tilde{\Phi} \equiv \frac{\overline{\rho\Phi}}{\bar{\rho}}$$

$$\Phi \equiv \Phi'' + \tilde{\Phi}$$

When the turbulent fluctuations lead to significant fluctuations in the density, this averaging process is more accurate. Such is the case for the models in the current study.

3.2 Turbulence

An exact definition on the phenomenon of turbulence is still elusive, but it is represented by the chaotic and unpredictable motions in flows. The effect of increased mixing and friction which leads to elevations in turbulence, has an important role in most engineering applications and needs to be accounted for, especially in safety engineering (increased mixing and friction of a flammable gas can lead to accelerated fire or explosion spreading).

When the Reynolds number of a laminar flow is increased sufficiently, the effect of turbulence arises with it. The disturbances in the laminar flow grow and take energy from

it, and can no longer be damped by the bulk. After the averaging procedure is applied on the Navier-Stokes equations to account for the effect of turbulence, new components emerge in the equations, known as the Reynolds stresses (τ_{ij}).

- $\tau_{ij} \equiv -\overline{\rho u'_i u'_j}$ for Reynolds averaging
- $\tau_{ij} \equiv -\overline{\rho u''_i u''_j}$ for Favre averaging

Such effect is the reason for the *closure problem*, the solution cannot be reached because there are more unknown parameters than the number of equations. This problem is still the subject of intense modelling and interest today. The use of a model that predicts the effects of turbulence is necessary to bypass this problem. There are three important model categories developed so far, with many branches and subcategories:

1. Direct Numerical Simulation models (DNS)
2. Reynolds-Averaged Navier Stokes models (RANS)
3. Large Eddy Simulation models (LES)

3.2.1 Direct Numerical Simulation

It was predicted by Andrei N. Kolmogorov in the middle of the 20th century that when the flow is highly turbulent, an energy-conserving cascade between the scales is present; the energy from the large-scale eddies is transferred to finer and finer scales until it is dispersed to heat. The DNS model resolves the Navier-Stokes equations for all the spatial and temporal scales of turbulence.

This implies that there is a requirement for vast grids in the computational domain of simulations, in order to effectively capture all scales. Even a simple case would require resources beyond the capability of the average modern machine. However, the solution would be extremely accurate.

This is why the DNS model is used mainly for the development and validation of other models. The fast-paced growth of technology may allow DNS simulations to be more frequently used in the near future.

3.2.2 Reynolds-Averaged Navier Stokes

As the title suggests, RANS models depend on the classical time (Reynolds) averaging that is demonstrated earlier. The models involve computation and modelling of the unknown Reynolds stresses that arise after the averaging process. This approach has been widely used due to its computational robustness, simplicity and a wide number of well-documented validation cases (Kumar and Dewan, 2014). RANS models are categorized depending on the extra variables that are added (Frei, 2013):

1. Zero equation model: Mixing length model

In this model only two parameters are considered in order to compute the turbulent viscosity, the local fluid velocity and the distance to the closest wall. This is the least computationally intensive method but also the least accurate, however it provides good approximations for the internal flow.

2. One equation model: Spalart-Allmaras

Originally developed for aerodynamics applications, this low-Reynolds number model adds a single additional variable for a Spalart-Allmaras viscosity and does not use any wall functions. It is quite stable and convergent but lacks accuracy when shear flow, separated flow or decaying turbulence is present.

3. Two equation models: k - ϵ style models

The k - ϵ models solve for two extra variables: k , the turbulent kinetic energy, and ϵ , the kinetic energy dissipation rate, while wall functions are present. These models are the most popular amongst industrial applications as they show good convergence and low computational costs. In cases with external flows around complex geometries these models perform well, but they lack accuracy in flow fields that exhibit adverse pressure gradients.

4. Seven equation model: Reynolds stress model

In the Reynolds stress model, the Reynolds stresses are directly computed using differential transport equations. The Reynolds-averaged momentum equation is solved

through a closure method, named *Second Order Closure*. They are the physically most complete models since history, transport and anisotropy of the turbulent stresses are all accounted for, but they require the most computational effort (less demanding than DNS though).

3.2.3 Large Eddy Simulation

Large Eddy Simulations are the principal subject of this project. In 1963, Joseph Smagorinsky proposed an alternative approach in simulating turbulent flows with high Reynolds numbers. In LES, the large scale motions (large eddies) of the turbulent flow are computed directly and only small scale (sub-grid scale (SGS)) motions are modelled, resulting in a significant reduction in computational cost compared to DNS. Roughly speaking, LES can be thought as a compromise between DNS and RANS. The LES is created through a filtering process, where the damping of the high frequency oscillations, either temporal or spatial, occurs by integrating the terms of the Navier-Stokes equations with a filter function (Worthy, 2003)(Zhiyin, 2015).

$$\phi(x) = \bar{\phi}(x) + \phi'(x)$$

where

$$\bar{\phi}(x) = \int_{\Omega} G_{\Delta}(x, y)\phi(y)dy$$

and G_{Δ} is the filter function (the indicator Δ is the filter width), which satisfies the normalization condition:

$$G_{\Delta}(x, y)dy = 1$$

The ones that are the most widely used are the top-hat, Gaussian and cut-off filters.

- $G(\text{top-hat}) = \begin{cases} \frac{1}{\Delta^3}, & -\frac{\Delta}{2} \leq |x| \leq \frac{\Delta}{2} \\ 0, & \text{otherwise} \end{cases}$
- $G(\text{Gaussian}) = \frac{\exp(-|x|^2/\sigma^2)}{(\sigma\sqrt{\pi})^3}$

$$\bullet \quad G(\text{cut-off}) = \begin{cases} 1, & |\kappa| \leq \kappa_c \\ 0, & \text{otherwise} \end{cases}$$

In this study, since the grids are uniform, the filter used is the grid filter and the filter width Δ is a measure of the local grid size. It is possible to calculate the filtered quantities from the filtered governing equations, to provide an approximation to the large-scale motions in the flow fields. Then the SGS stress terms which represent the influence of SGS motions are modelled in terms of resolved quantities.

3.2.4 Effects of turbulence

The size of the smallest structures in the turbulent flow can be estimated with the use of dimensional analysis as follows:

$$\frac{\eta}{l} \sim Re_l^{-3/4}$$

where η is the Kolmogorov length, l is the largest length scale and Re_l is the Reynolds number based on l . Kolmogorov microscales represent the smallest scales in turbulent flow for length, time and velocity. The Kolmogorov length scale η is equal to:

$$\eta = \left(\frac{\nu^3}{\epsilon}\right)^{1/4}$$

The choice of the turbulence model strongly depends on the particular case and its characteristics, along with the desired level of detail. A demonstration of the level of prediction for each turbulence model discussed is summarized in Figures 3.1 and 3.2.

The turbulent kinetic energy is distributed across the eddies' physical length scales, which correspond in wavenumbers in Fourier space. Based on Kolmogorov's hypothesis, the energy content of turbulence is dependent only on the rate of energy dissipation, ϵ , at which the smallest scales of turbulence convert motion into heat and the wavenumber κ (proportional to the inverse of the eddy lengthscale). This implies that turbulence behaves in an isotropic fashion, a fact that has much bearing on the practicalities of LES (De Villiers, 2006). Since the energy contained in the wavenumber represents the energy of an eddy of a certain size, an approved way of monitoring turbulence is through the energy spectrum,

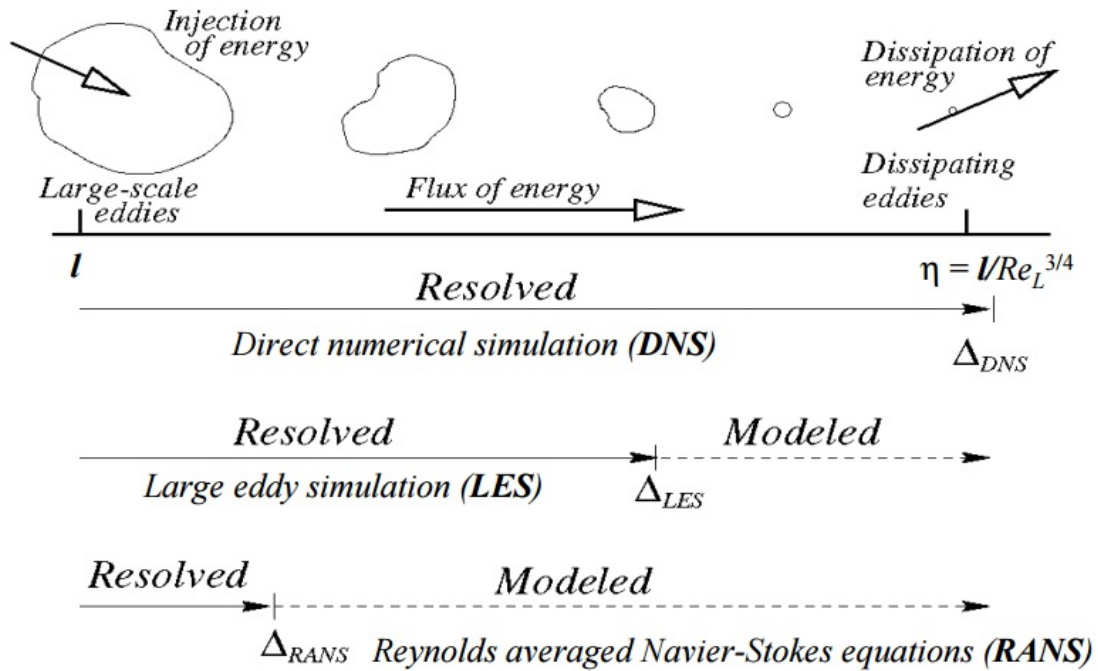


Figure 3.1: Resolution levels of DNS, LES, RANS methods (figure adapted from CFD lecture material at Dartmouth College, USA (2006)).

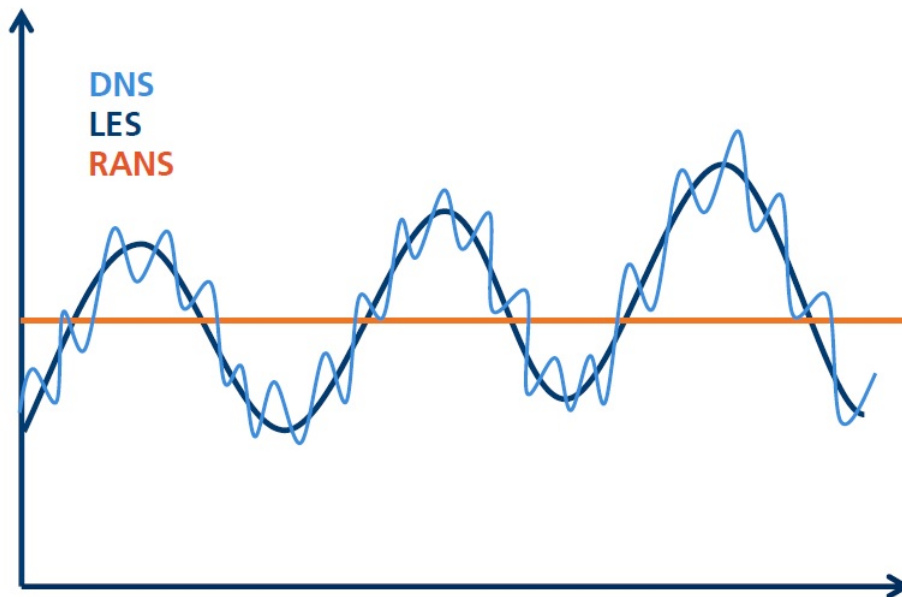


Figure 3.2: Comparison of the simulation detail levels between DNS, LES, RANS methods (figure from CFD course material at the University of Stavanger, Norway (2017)).

which acts as a graphical expression of Kolmogorov's law. This can be obtained by the integral across Fourier space of the energy in different wavenumbers.

As Kolmogorov suggested, the energy spectrum can be described as a function of ϵ and κ . Derived through dimensional reasoning, an expression for it can be reached (Davidson, 2017):

$$E = \kappa^\alpha \epsilon^\beta \quad (3.7)$$

Since the physical meaning of E is kinetic energy per unit wavenumber of eddies of size κ^{-1} , the units are that of $u^2/\kappa \sim (m^3/s^2)$. κ is the inverse of the eddy lengthscale so the units are m^{-1} , and the dissipation rate ϵ has units (m^2/s^3) .

$$(m^3/s^2) = (1/m)(m^2/s^3)$$

Adapting into equation (3.7), there are two new equations, one for meters (m) and one for seconds (s).

- (m): $3 = -\alpha + 2\beta$
- (s): $-2 = -3\beta$

By inserting α , β into (3.7), the following expression is produced:

$$E(k) = C_k \epsilon^{2/3} k^{-5/3} \quad (3.8)$$

where C_k is the Kolmogorov constant, with experimental values that range in $1.4 \sim 1.6$.

Equation (3.8) is the so-called -5/3 law, where fully turbulent flows exhibit a -5/3 decay in the inertial region, as it is demonstrated in Figure 3.3.

The main sections of an idealised energy spectrum can be summed up in the following:

1. The energy containing scales, where turbulent energy is introduced to the system. These scales contain the most turbulent kinetic energy by far and their motions are unstable but with permanent character.
2. The inertial subrange, where Kolmogorov's law describes the scales which are dominated by inertial forces rather than viscosity. Only small amounts of turbulent kinetic

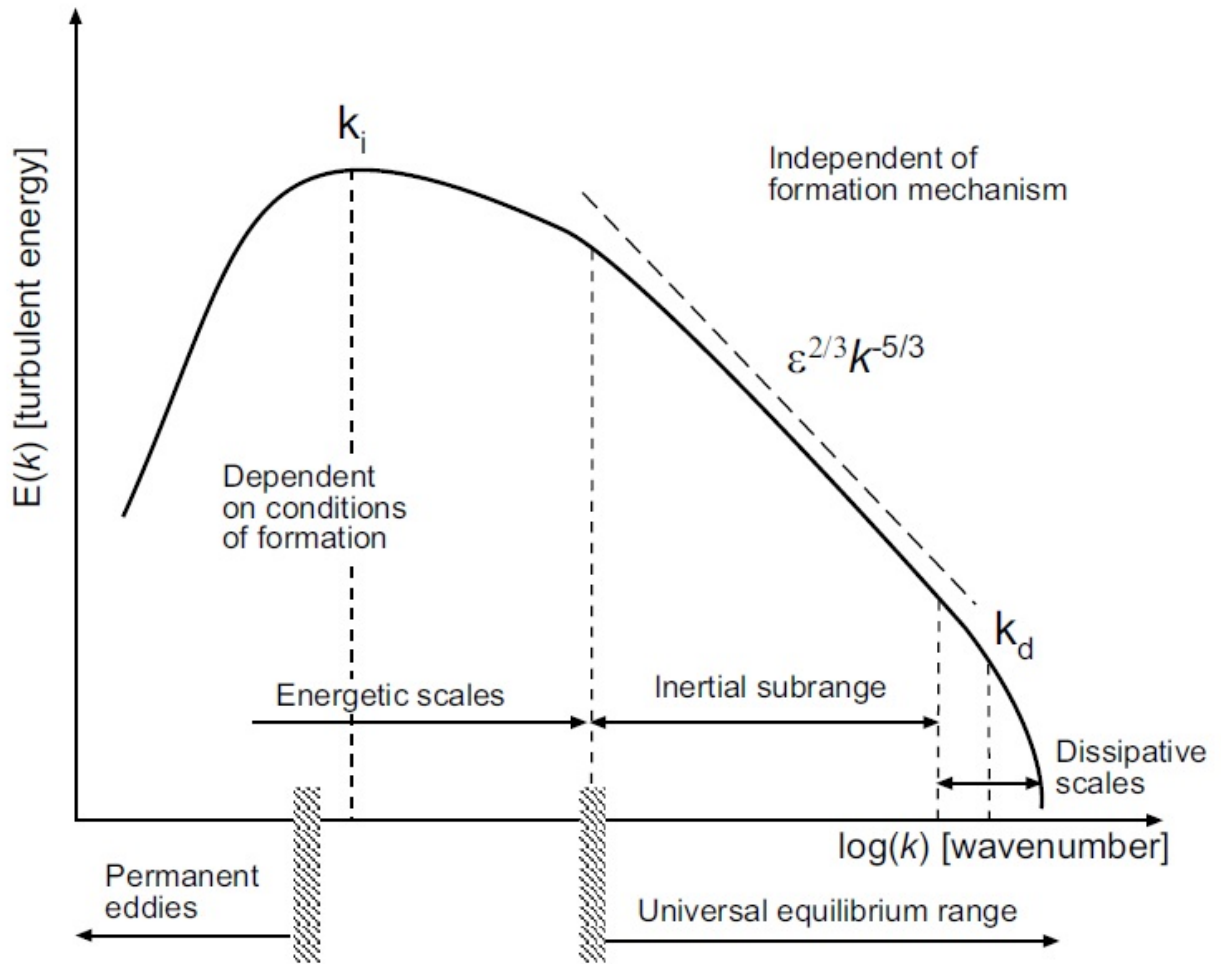


Figure 3.3: Three dimensional flow topologies (figure adapted from De Villiers (2006)).

energy is contained in these scales.

3. The dissipative range, with scales of motion smaller than the Kolmogorov length scale $\kappa_d \propto 1/\eta = (\epsilon/\nu^3)^{1/4}$, where effects of viscosity are superior to turbulent motions.

The universal equilibrium range consists of the inertial subrange along with the dissipative range. There the turbulence is considered to be fully developed and independent from forcing effects and boundary conditions.

3.3 Adaptation to current study

For the weakly compressible flows of this study, after applying the density-weighted Favre averaging, the spatially filtered Navier-Stokes equations for continuity (3.9), momentum (3.10) and energy conservation (3.11) take the following form, identical to the ones illustrated by Zhou et al. (2001). Including the expressions for Reynolds, Froude and Prandlt numbers would give the conservation equations forms similar to the ones presented in Pham (2007) for DNS (without the spatial filtering). However, in an effort to reduce the extent of the inserted parameters and definitions and highlight the focus on the LES model evaluation, the illustration of Zhou et al. (2001) is indicated:

$$\frac{\partial \bar{\rho}}{\partial t} + \frac{\partial(\bar{\rho}\tilde{u}_j)}{\partial x_j} = 0 \quad (3.9)$$

$$\frac{\partial(\bar{\rho}\tilde{u}_i)}{\partial t} + \frac{\partial(\bar{\rho}\tilde{u}_i\tilde{u}_j)}{\partial x_j} = -\frac{\partial\bar{p}^{(1)}}{\partial x_i} + \frac{\partial\bar{S}_{ij}}{\partial x_j} + (\rho_\alpha - \bar{\rho})g_i - \frac{\partial\tau_{ij}}{\partial x_j} \quad (3.10)$$

$$\frac{\partial(\bar{\rho}\tilde{h})}{\partial t} + \frac{\partial(\bar{\rho}\tilde{u}_j\tilde{h})}{\partial x_j} = \frac{\partial}{\partial x_j} \left[\left(\frac{k}{c_p} \right) \frac{\partial\tilde{h}}{\partial x_j} \right] - \frac{\partial Q_j}{\partial x_j} \quad (3.11)$$

Where \tilde{u}_i and \tilde{h} are the Favre-filtered velocity and enthalpy respectively, for which:

$$\tilde{u}_i = \frac{\overline{\rho u_i}}{\bar{\rho}}, \tilde{h} = \frac{\overline{\rho h}}{\bar{\rho}}$$

The density of the ambient air is ρ_α , and $p^{(1)}$ is the hydrodynamic pressure. To account for the buoyancy effect, the gravitational force term, g_i , is included along the negative vertical direction. For the subgrid scales, the parameters that require closure models are the following:

- SGS Reynolds stress: $\tau_{ij} = \overline{\rho u_i u_j} - \overline{\rho} \tilde{u}_i \tilde{u}_j$
- SGS heat flux: $Q_j = \overline{\rho u_j h} - \overline{\rho} \tilde{u}_j \tilde{h}$

While the molecular strain rate tensor is given by:

$$\overline{S}_{ij} = -\frac{2}{3}\mu \frac{\partial \tilde{u}_k}{\partial x_k} \delta_{ij} + \mu \left(\frac{\partial \tilde{u}_i}{\partial x_j} + \frac{\partial \tilde{u}_j}{\partial x_i} \right)$$

The cascade of energy from the large to the small scales is represented by the SGS terms. The SGS terms cannot be calculated and require closure models, and there has been a number of such models developed with LES in OpenFOAM and KFX.

3.3.1 LES model in OpenFOAM®

The turbulence model selected in the OpenFOAM simulations is denoted "dynamicKEqn", which represents the dynamic one-equation eddy viscosity SGS model. This model is based on the work of Kim and Menon (1995), progressing from the initial approach of Germano (1991). Several models with slight changes to that have been produced in recent years (Chai and Mahesh, 2012), (Huang and Li, 2010).

This type of model obtained its name by using a transport equation for the SGS kinetic energy coupled with the dynamic formulation. Even though the initial model introduced by Germano (1991) had been successfully applied to a various types of flow fields, it faced some significant drawbacks. It is based on the Smagorinsky's time-independent, algebraic eddy viscosity model, the assumption for which is that there is a local equilibrium between the SGS energy production and dissipation rate. This is the result of an independent relation which is used to close the model, as the expressions for the SGS stress tensors and dissipation rates contain two unknown model coefficients. Thus, the neglect of the non-local and history effects of the turbulence evolution is unavoidable.

To overcome this, Kim and Menon (1995) proposed a new approach, where the coefficient c_t in the SGS stress tensor expression at the grid filter level τ_{ij} and the coefficient c_e in the SGS dissipation rate e_{SGS} are related in an expression that does not contain additional unknowns. The dynamic modelling approach is obtained by resolving the stresses between the grid scale filter of length $\bar{\Delta}$ and a test filter of length $\hat{\Delta}$ to determine the model coefficient. In most cases the length of the test filter is the double of the grid filter ($\hat{\Delta} = 2\bar{\Delta}$). The formal illustration follows:

$$c_t = \frac{1}{2} \frac{t_{ij} \sigma_{ij}}{\sigma_{ij} \sigma_{ij}} \quad (3.12)$$

where

$$\sigma_{ij} = -\hat{\Delta} \left[\frac{1}{2} (\langle \bar{u}_i \bar{u}_i \rangle - \hat{u}_i \hat{u}_i)^{\frac{1}{2}} \hat{S}_{ij} \right] \quad (3.13)$$

$$c_e = \frac{\nu (\langle \frac{\partial \bar{u}_i \partial \bar{u}_i}{\partial x_j \partial x_j} \rangle - \frac{\partial \hat{u}_i \partial \hat{u}_i}{\partial x_j \partial x_j})}{[\frac{1}{2} (\langle \bar{u}_i \bar{u}_i \rangle - \hat{u}_i \hat{u}_i)^{\frac{3}{2}} / \hat{\Delta}}] \quad (3.14)$$

The math mode accents $\hat{\phi}$ and $\langle \phi \rangle$ symbolize the variable ϕ to which the test filter of the model is applied. Other test filter terms include $\hat{\Delta}$, the length scale, and \hat{S}_{ij} the strain rate. Parameter t_{ij} represents the SGS stress tensor at the test filter level. The denominators of the equations (3.12), (3.14), take into account the energy on the resolved scale. Additional advantages of this model are the relatively cheap computational cost, robustness and its efficiency in actual numerical implementations.

3.3.2 LES model in KFX®

As it was mentioned in section 3.2.3, the filtering process of the LES methods can be applied to either temporal or spatial oscillations. The LES turbulence model that KFX utilizes is based on the temporal filtering of the Navier-Stokes equations. An illustration of this approach has been well documented in the work of Pruett (2003), which is demonstrated later on this section.

The RANS turbulence models depend on the long-time averaging of the Navier-Stokes equations, and are good for modelling statistically steady flows. However, this methodology is not used for more complex flows as it is difficult to model the Reynolds-stress tensors

because they incorporate the effects of all the unsteady motions upon the mean.

A linkage between LES and RANS methodologies was established by Germano (1999), where both filtering and averaging procedures are combined to reach a consistent solution. It is believed that this linkage has a more natural character, within the context of time-domain, than the spatial filtering that is commonly used in other LES methods.

This methodology is illustrated in the work of Pruett (2003), where the time-domain filters the continuous function of time $f(t; \Delta)$.

$$\bar{f}(t; \Delta) = \int_{-\infty}^t G(\tau - t; \Delta) f(\tau) d\tau$$

where G is the filter kernel, Δ is the filter width and the parameter τ is the preassigned time value which filters the domain.

After the filtering process, the Temporally Filtered Navier-Stokes (TFNS) equations obtain the following form:

$$\frac{\partial \bar{u}_j}{\partial x_j} = 0 \quad (3.15)$$

$$\frac{\partial \bar{u}_i}{\partial t} + \frac{\partial (\bar{u}_i \bar{u}_j)}{\partial x_j} = -\frac{\partial \bar{p}}{\partial x_i} + \nu \frac{\partial^2 \bar{u}_i}{\partial x_j \partial x_j} - \frac{\partial [\tau_R]_{ij}}{\partial x_j} \quad (3.16)$$

The quantities that are being temporally filtered are represented by the overbar, while parameter $[\tau_R]_{ij}$ in equation (3.16) defines the temporal residual stress tensor:

$$[\tau_R]_{ij} \equiv \overline{u_i u_j} - \bar{u}_i \bar{u}_j$$

It has been proven that the residual stress of the TFNS equations depends heavily on the temporal filter width. The smaller the value of the temporal filter width, the TFNS equations approach the DNS ones. That means that this approach gains more accuracy but also increases its computational cost. A finite filter width describes a temporally filtered LES method.

Chapter 4

Thermal Plume

The first case of interest is the thermal plume, as it has been extensively studied by Kumar and Dewan (2014), Dai et al. (1995), Shabbir and George (1994), Zhou et al. (2001), Pham (2007) and it has been the subject of focus for the PhD thesis of Worthy (2003). The actual experiment involves the injection of a fluid with high temperature into the ambient air, without a chemical reaction taking place. The turbulent flow is dominated from buoyancy, and it can be encountered in diverse applications:

- Spreading of fire, smoke and other pollutants into the atmosphere.
- Vertical motion of air into the atmosphere.
- Dispersal of volcano exhaust and water outfalls.
- Space heating and cooling.
- Nuclear reactor containment.
- Solar collectors.

Turbulent thermal plumes are described by the relation between the momentum of fluid motion and the buoyancy force developed by the thermal energy transport. The latter has the biggest impact on the turbulence generation.

This chapter focuses on the domain size, geometry, grid scale and other characteristics that describe the simulation of a buoyant thermal plume, and the collected results. There

are numerous scientific references available regarding this case, and experimental data were obtained from the literature. As it will be demonstrated, there are some significant differences in the development of the thermal plume between OpenFOAM and KFX.

4.1 Computational setup

The geometry of the thermal plume case is considered simple, as the inlet boundary is represented by a circular source at the bottom of the domain (Figure 4.1). The diameter D of the source is 6.35 cm, and the hole domain covers an area of $6D$ in the x,y direction, and $16D$ in the z direction. The hot air inlet is injected through the bottom source with an initial velocity of 0.98 m/s, and a temperature of 565 K. The ambient temperature inside the domain is at 300 K, and the pressure p is stable everywhere at 101325 Pa.

The inflow conditions are the same as the ones used by Shabbir and George (1994), from which case the experimental data are also collected. For the TFNS model, the turbulent kinetic energy k is specified at $3.602 \cdot 10^{-5} \text{ m}^2/\text{s}^2$, and the turbulent dissipation rate ϵ at $8.389 \cdot 10^{-6} \text{ m}^2/\text{s}^3$.

In the OpenFOAM environment, two different uniform mesh grids are initially applied for each simulation software in this experiment. The mesh consists of rectangular cells of similar dimensions. This is performed to assess the impact of the grid on the accuracy of the simulation, and to further validate the correct implementation of the computational approach. KFX version has different cells that are slightly longer in the z direction. However, as it will be demonstrated and discussed in detail later on, the differences in the results from the two grids are very slight. Therefore, having initially conducted the OpenFOAM simulations, it is decided to run the simulations only for the coarse grid in KFX.

The characteristics of the simulations, including domain size L , number of cells N , cell sizes Δ , time steps Δt and simulation time τ are summarized in Table 4.1.

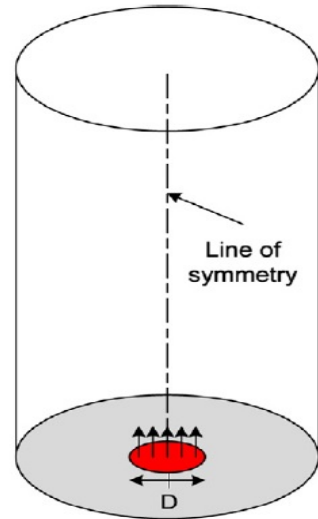


Figure 4.1: Illustration of the domain (Kumar and Dewan, 2014).

Table 4.1: Characteristics of the thermal plume simulations.

Case	OpenFOAM coarse grid	OpenFOAM fine grid	KFX grid
$L_x \times L_y \times L_z$ (m)	$0.381 \times 0.381 \times 1.016$	$0.381 \times 0.381 \times 1.016$	$0.381 \times 0.381 \times 1.016$
$N_x \times N_y \times N_z$	$46 \times 46 \times 123$	$92 \times 92 \times 246$	$51 \times 51 \times 130$
$\Delta_x \times \Delta_y \times \Delta_z$ (m)	$(8.3 \times 8.3 \times 8.3) \times 10^{-3}$	$(4.1 \times 4.1 \times 4.1) \times 10^{-3}$	$(7.4 \times 7.4 \times 7.8) \times 10^{-3}$
Δt (s)	2×10^{-3}	2×10^{-3}	2×10^{-3}
τ (s)	60	30	30

4.2 Simulation with OpenFOAM®

OpenFOAM environment requires a set of parameters to be adjusted in the input files before proceeding with the simulation. The initial case directory contains 3 files.

- 0
- constant
- system

The file "0" includes all the information about the initial conditions in the boundary fields for the main parameters of the simulation, and what conditions will be followed during the course of the simulation. There the initial field values for u, T, p, k, ϵ are inserted along with the boundary conditions.

The "constant" file contains the dictionaries for the polymesh, the thermophysical and the turbulence properties of the case. In polymesh all the details of the mesh are defined, like the geometry characteristics, the dimensional points and faces of the cells and the boundary areas. The thermodynamic and physical properties of the mixture are also defined inside the "constant" file. In addition to these, the turbulence model is selected here, along with the necessary coefficients. Regarding the current case, the dynamic one-equation eddy viscosity turbulence model is selected, but the supporting coefficients (Prandtl, van Driest) are not relevant, since they are used for near-wall modelling which is not the case of the current geometry.

In the last file named "system", the necessary information for the structure of the geometry and the grid, the duration of the simulation along with the time step, the numerical schemes for terms calculated during the simulation and the equation solvers and algorithms

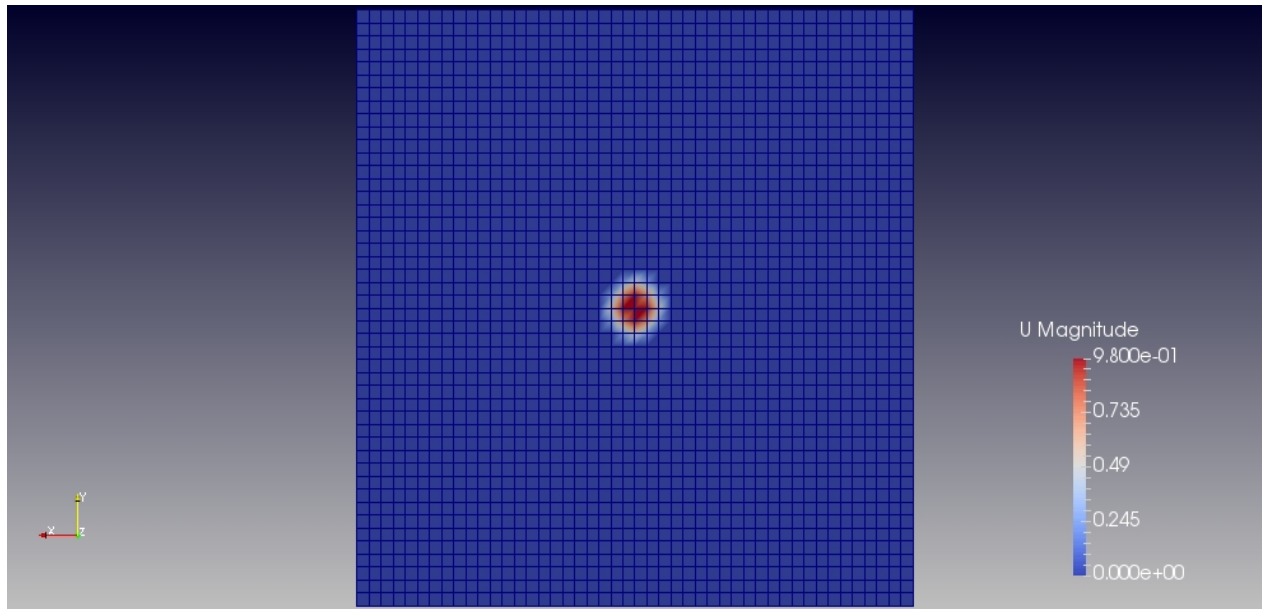


Figure 4.2: Snapshot of the initial conditions on the ground surface.

are contained. In addition to that, the method for fragmenting the simulation domain into different components (decomposition method) is defined, in order to use multiple processors and enhance the overall speed. After adjusting all the parameters, the initial conditions of the domain are presented in Figure 4.2.

4.2.1 OpenFOAM solver

OpenFOAM relies on the *finite volume method*, utilizing several numerical schemes and solvers to compute the algorithms for the closure of the Navier-Stokes equations. For heat transfer and buoyancy driven flows of compressible fluids, the transient solver to use is called "*buoyantPimpleFoam*". PIMPLE is a large-step transient merged version of PISO (Pressure Implicit with Splitting of Operators) and SIMPLE (Semi-Implicit Method for Pressure-Linked Equations) algorithms, which are a transient solver and a steady-state solver for incompressible turbulent flow, respectively. Since LES models require small time steps, the SIMPLE part of the algorithm is not utilized. This version accounts for the weakly compressible characteristics of the buoyancy.

4.2.2 Turbulence model

The turbulence model selected is denoted "dynamicKEqn", which represents the dynamic one-equation eddy viscosity SGS model. As explained analytically in section 3.3.1, this model is based on the work of Kim and Menon (1995), progressing from the initial approach of Germano (1991). This type of model obtained its name by using a transport equation for the SGS kinetic energy coupled with the dynamic formulation.

4.2.3 Boundary conditions

In order to effectively capture the development and evolution of turbulence, the use of the "turbulentInlet" function for the velocity is utilized. As the inflow conditions are close to laminar flow conditions, the transition to turbulent flow is not handled by the LES method. This function inserts random fluctuations of the velocity in x,y,z directions, as a fraction of the mean value. This is a simple approach without a strong physical explanation, as it does not account for the temporal and spatial structures in turbulence. It is represented by the following function (OpenFOAM, 2013):

$$x_p = (1 - \alpha)x_p^{(n-1)} + \alpha(x_{ref} + sC_{RMS}x_{ref}) \quad (4.1)$$

where,

- x_p are the patch values.
- x_{ref} are the reference patch values.
- n is the time level
- α is the fraction of a new component added to the previous time value.
- C_{RMS} is the RMS coefficient.
- s is the fluctuation scale.

The parameters that are required to be inserted in this condition are the fluctuation scale, s , which in this case was chosen at 0.5 in x,y,z directions, and the reference field, x_{ref} ,

which is 0.98 m/s in the z direction. Parameter α does not necessarily need to be adjusted, so it is considered with a value of 1.

This noise amplitude, in the form of the generated random fluctuations, is necessary to render possible a transition process of the flow field to turbulence away from the source (Pham, 2007), and has been documented in previous work relevant with thermal plume simulations. The remaining boundary conditions are considered as thermally and dynamically passive flow conditions.

4.3 Simulation with KFX®

The KFX software is dedicated to simulating gas dispersions, flares and fires for consultancy services in safety engineering. It includes a tool named "KFX doozer" for creating the 3D geometry, but there is also the option for importing CAD files.

The geometry of this case was designed in Doozer, declaring the commands at the left of the screen as presented in Figure 4.3 to design the domain of $6D \times 6D \times 16D$, with the circular source at the bottom. The mesh grid and the boundary areas are specified afterwards, in the main interface of KFX.

The domain size is set with points in the x,y,z directions, and the grid is adjusted to uniform with the cells (grid nodes) generated automatically after the grid node size is specified, according to the data shown in Table 4.1. The domain and boundary records are inserted according to the ones specified in section 4.1.

4.3.1 Parameter setup

An important detail that must be mentioned, because KFX is mainly used for fire simulations, is that a composite fuel formula must be selected in order to use KFX. This cannot be applied in the current case, as the composite fuel formula for hot air cannot be used. To overcome this, the fuel $C_2H_{4.5}$ is selected in a low concentration because it has almost the same density with air at 565 K ($\sim 0.61 \text{ kg/m}^3$). So the actual mixture is composed of 0.79 N_2 , 0.2099 O_2 and 0.0001 $C_2H_{4.5}$, instead of 0.79 N_2 , 0.21 O_2 and zero $C_2H_{4.5}$.

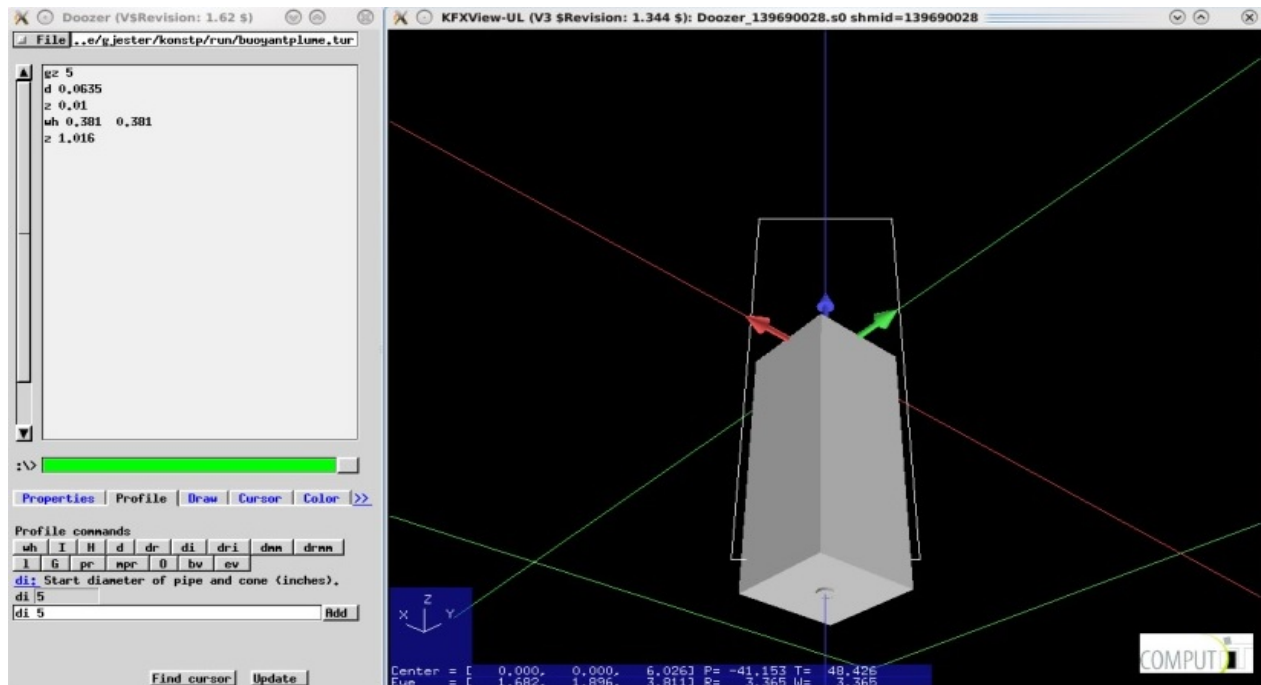


Figure 4.3: KFX doozer interface.

KFX includes its own automated discretization methods to be used as solvers for the transport equations, based on Gaussian elimination algorithms that will not be analyzed here. The time step is set to a value identical to the OpenFOAM version (2×10^{-3}), while the difference here is that a value must be set for the temporal filter of the Navier-Stokes equations. As it was mentioned in section 3.3.2, this LES model implements a temporal filter width, and when its value approaches zero the TFNS equations approach the DNS ones. Here the value of the filter is set to 0.05 seconds, which, given the size of the eddies in the domain, is an appropriate value. The $k-\epsilon$ model is filtered so that eddies with time scale larger than this value are solved by the Navier Stokes solver.

The noise amplitude in the inlet that is applied in the OpenFOAM simulations cannot be inserted here, as KFX does not provide a function for that yet. Therefore, the velocity is set to a constant rate of 0.98 m/s in the z direction.

4.4 Results

All results are extracted through an averaging process, which begins when the quasi-steady state assumption (pseudo steady state) takes place. This assumption for steady state is applied when one part of the system equilibrates faster than the other. In the current cases, after 10 seconds of simulation time quasi-steady state is assumed. The writing interval for saving data is 1 second, so the total averaging takes place from 10 seconds up to the total simulation time for each case. Direct comparison with experimental data, which are averaged over a very large time period, is more accurate with this process.

For the thermal plume, results include axial velocity and temperature data, which are averaged in time during the quasi-steady state. The numerical along with the experimental results are placed in the same figures for direct comparison, from the most accurate simulation efforts. The kinetic energy spectrum is also calculated for the thermal plume case, to be used in validating the LES implementation as discussed in section 3.2.4.

The numerical results for the thermal plume collected from OpenFOAM and KFX simulations are compared to the experimental data from Shabbir and George (1994). As mentioned in section 3.1, there are 2 different grids generated for the OpenFOAM environment, but only the results from the coarse grid are presented here as the difference is minimal, as it will be proven in the Discussion chapter (section 7.2). Figure 4.4 contains a surface representation of the velocity magnitude in KFX at 20 seconds simulation time. Snapshots of the velocity magnitude at 30 seconds simulation time are presented in Figures 4.5 and 4.6, for all grids in OpenFOAM and KFX, respectively.

In Figure 4.7, the centerline averaged axial velocity (m/s) measurements are plotted against the distance from the source z/D , where D is the source diameter (0.0635 m) and the domain has a total height of $16D$. Inlet velocity has a value of 0.98 m/s.

Figure 4.8 includes the results for the centerline averaged temperature (K) against the distance from the inlet source, measured in the same dimensions (z/D) as for the centerline averaged axial velocity. Inlet temperature has a value of 565 K, and the experimental data were collected at the same points for both velocity and temperature.

The kinetic energy spectrum displayed in Figure 4.9 follows the $-5/3$ law (Equation

3.8), illustrating the decay slope of the energy from the larger to the smaller eddy scales. To develop the spectrum in OpenFOAM, function object "probes" is used to place points along the centerline to track the axial velocity. Then a Fast-Fourier transform in the data is performed for the transition in spectral space. The -3 slope accounts for buoyancy effects.

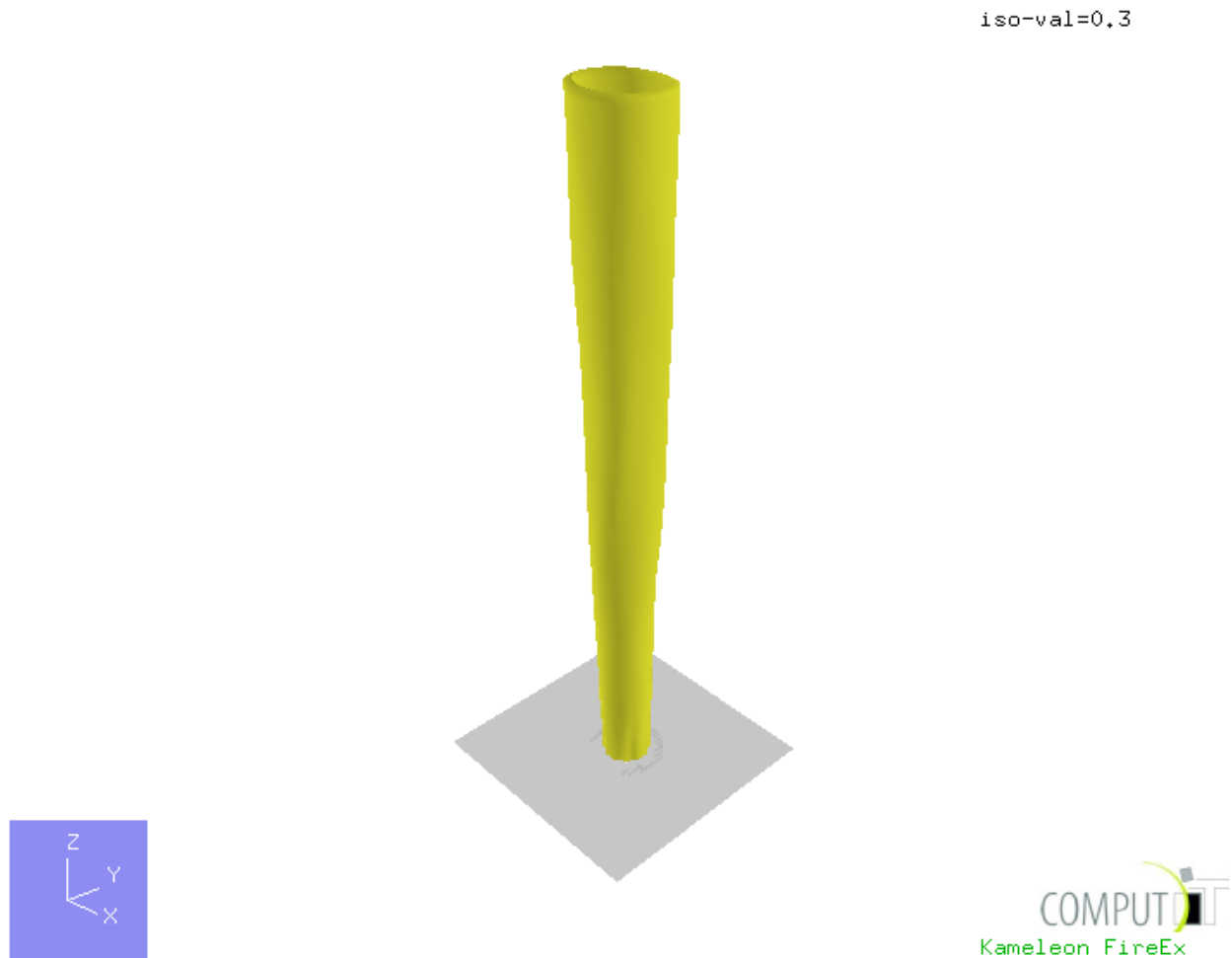


Figure 4.4: Development of the plume after 30 seconds simulation time in KFX, with an iso-surface value of 0.3.

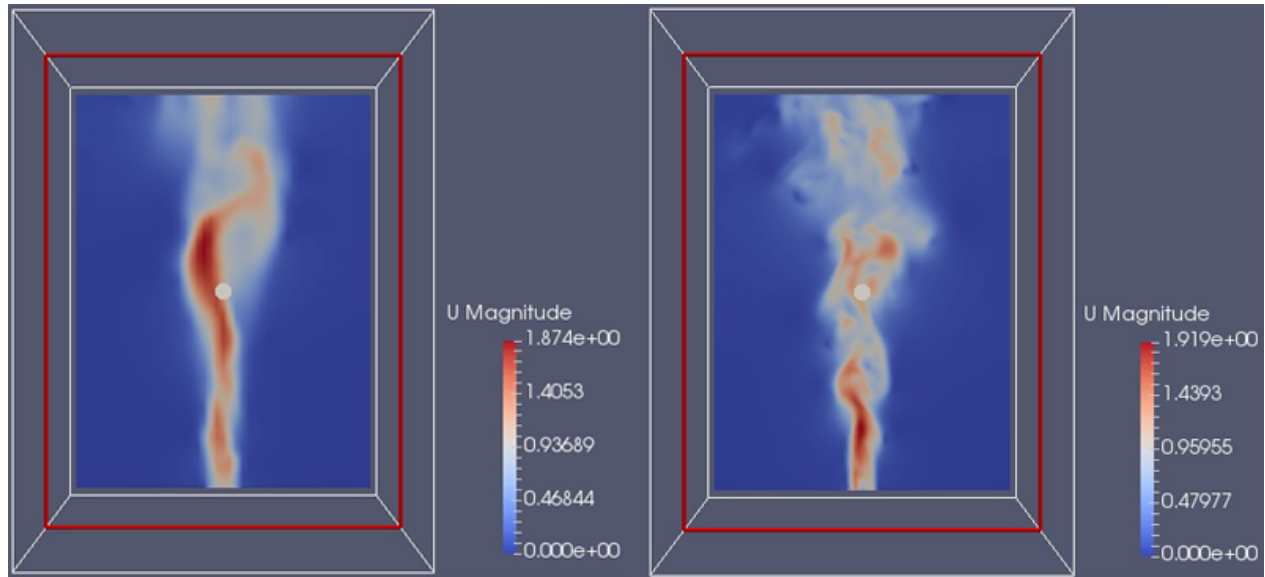


Figure 4.5: Snapshots of the axial velocity magnitude taken at 30 seconds simulation time on a slice of the domain at the center of the geometry in OpenFOAM, for the coarse (L) and the medium (R) grid. The variation of the detail between the grids is visible.

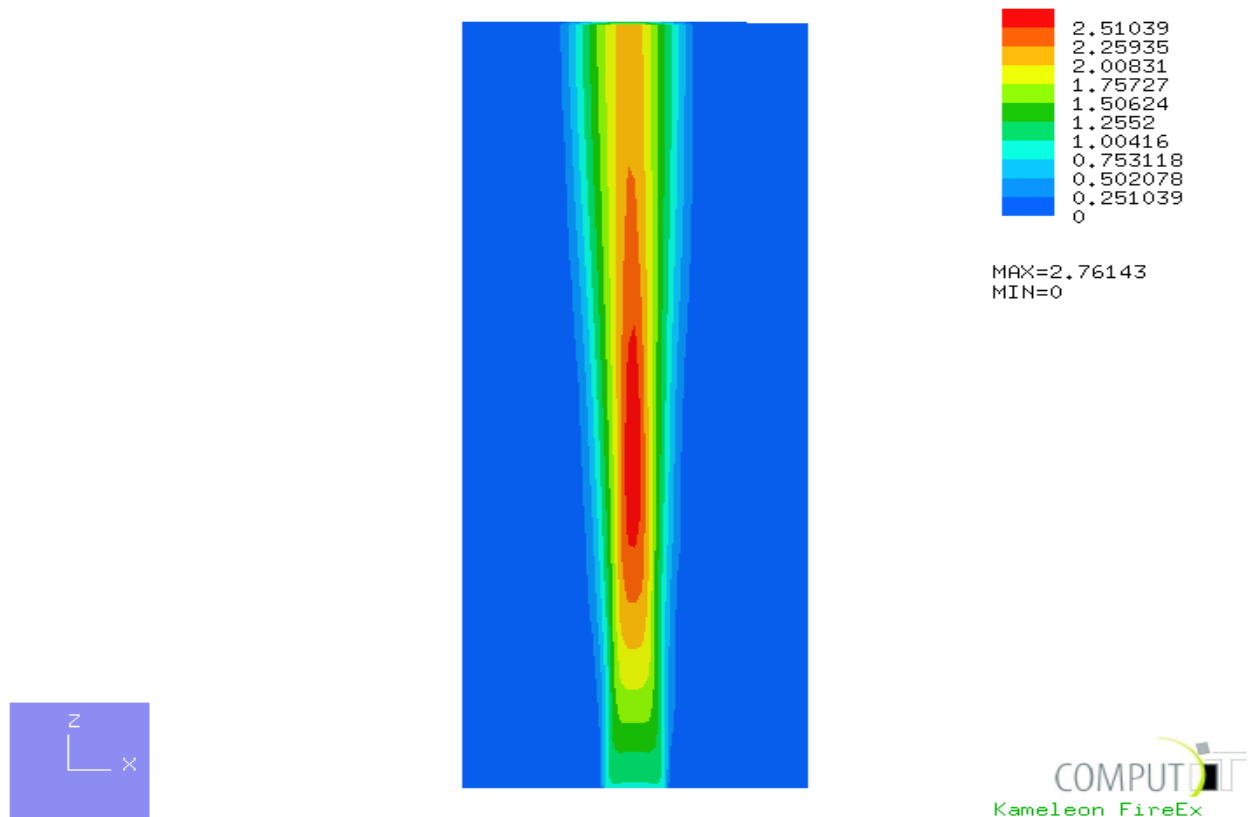


Figure 4.6: Snapshot of the axial velocity magnitude taken at 30 seconds simulation time on a slice of the domain at the center of the geometry in KFX.

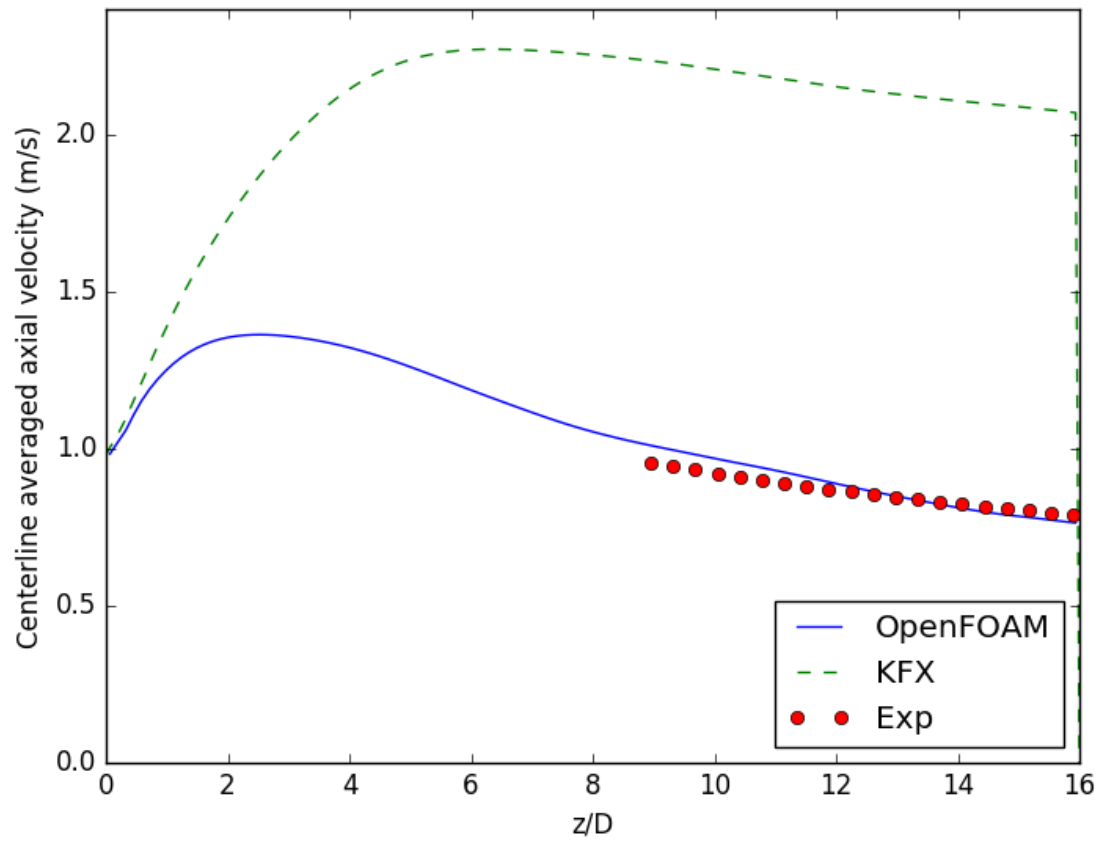


Figure 4.7: Centerline averaged axial velocity against the distance from the source for the thermal plume ($\tau = 30$ s).

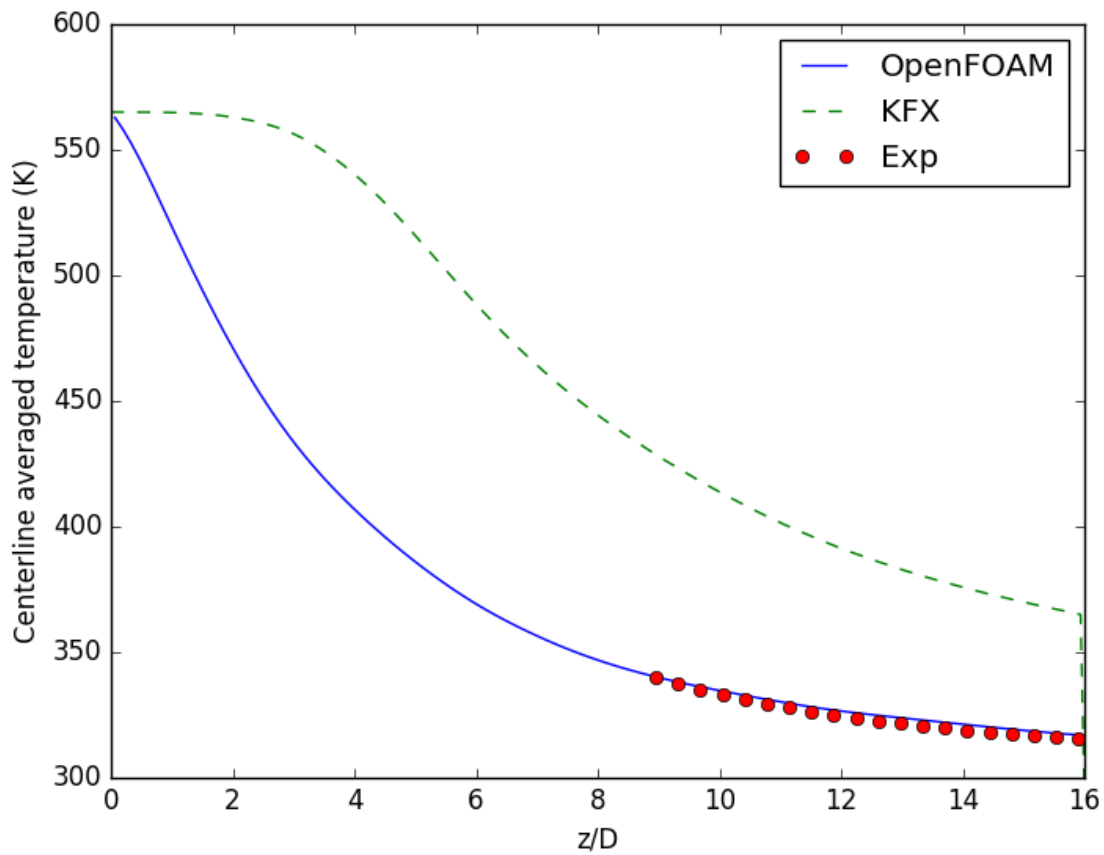


Figure 4.8: Centerline averaged temperature against the distance from the source for the thermal plume ($\tau = 30$ s).

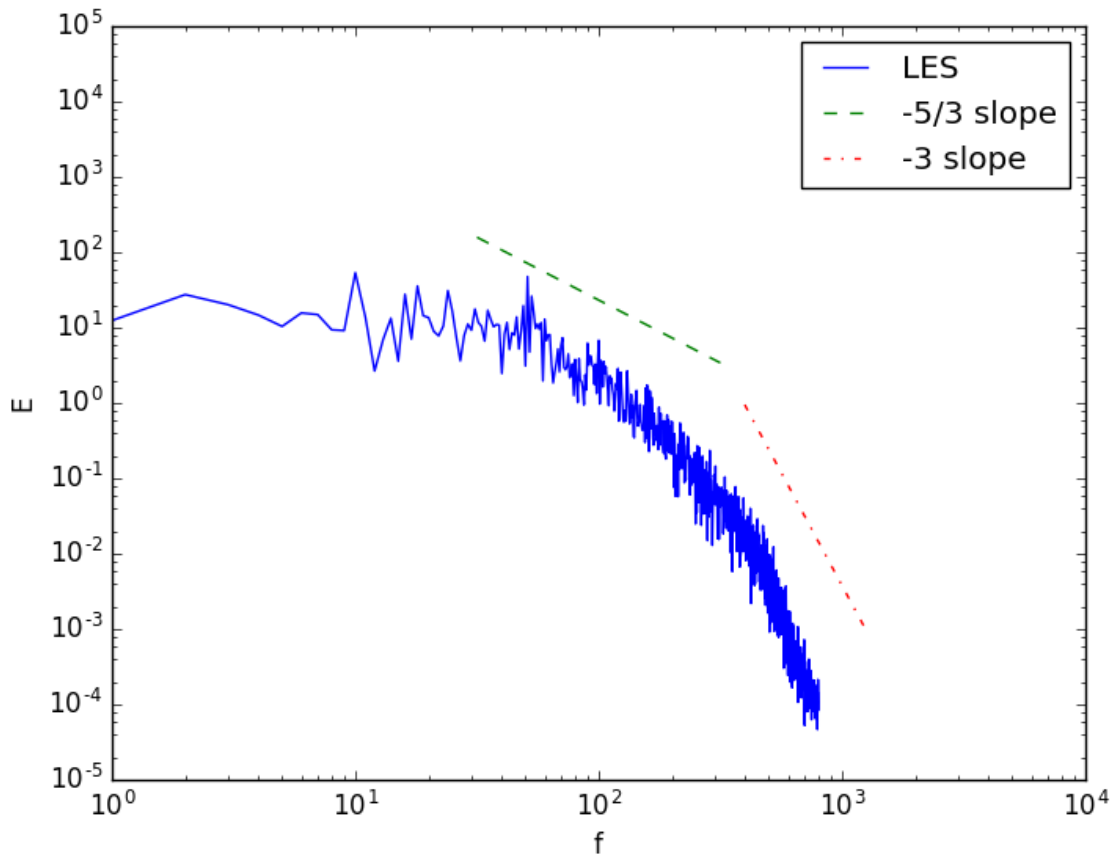


Figure 4.9: Turbulent kinetic energy spectrum for the thermal plume in OpenFOAM ($\tau = 30$ s).

Chapter 5

Helium Plume

The second case that has been studied is the one of the helium plume. Relevant literature by Chung and Devaud (2008), Blanquart (2008) and the Master's thesis of Chung (2007) have focused on the dispersion of helium into the ambient atmosphere. It is also a buoyancy-driven flow, but due to the lower-than-air density of helium instead of the high temperature of the injected fluid, which was the case for the thermal plume. Here, the density stratification between the heavy fluid on top of the light fluid, with the presence of gravity, makes the plume unstable and subject to Rayleigh-Taylor instabilities. This kind of instabilities in the interface between two fluids of different densities occur when the heavier fluid is being pushed by the lighter fluid. Some examples of this phenomenon can be noticed in the following:

- Gas dispersion of light gases, such as hydrogen and methane.
- Water suspended above oil.
- Mushroom clouds from atmospheric nuclear explosions.

In such flows velocity and density fluctuations initially appear at the small scales, and then continue to grow in size and magnitude which makes them able to interact eventually with the large-scale motion of the turbulent flow. Toroidal vortices are observed in many experiments of helium-air plumes which result in periodic oscillations called puffs. Studies focus on comparing the puffing frequencies to different parameters such as ambient pressure or exit velocity.

5.1 Computational Setup

The numerical parameters were set accordingly to the work of Tieszen (2005), from which the experimental data were also collected. An illustration of the domain is presented in Figure 5.1.

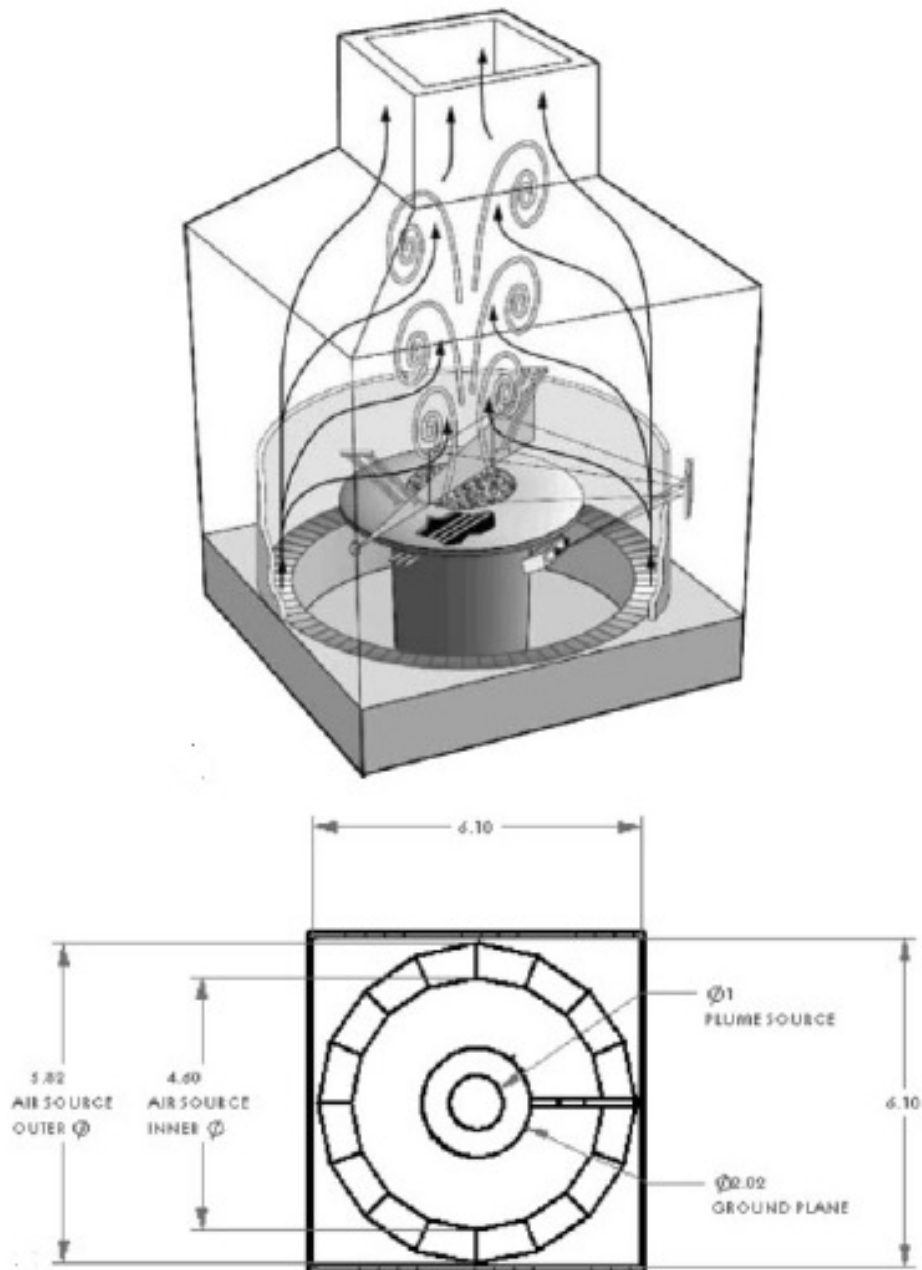


Figure 5.1: Structure of the helium experiment (figure adapted from Chung and Devaud (2008), relating to the setup of Tieszen (2005)).

The plume source is located inside a cubical enclosure of 6.1 m length, and a chimney on top of the chamber with a diameter of 2.3 m. The diameter D of the plume source is 1 m, located 1.74 m above the air duct. The experiment was conducted with acetone into the helium flow to be used as the fluorescent tracer gas, at 1.7 vol%. To quench the acetone phosphorescence, an air source (oxygen at 1.9 vol%) is also located below the helium inlet. However, this is believed not to affect the turbulence generation in the plume, along with the source height, so in OpenFOAM simulations it is not included. In KFX, the original case conducted by ComputIT included all parts of the geometry, but the restructured case for this study does not include the air inlet either.

The domain covers an area of $4D$ in the x,y directions and $16D$ in the z direction for OpenFOAM, and $6D$ in the x,y with $14D$ in the z for KFX. The helium plume has a molecular weight of 5.45 g/mol, and enters the chamber with a velocity of 0.325 m/s. The Reynolds number is equal to 3200 under these conditions. Temperature and pressure are stable at 300 K and 101325 Pa respectively, while turbulence parameters k and ϵ are set to $0.0001 \text{ m}^2/\text{s}^2$ and $0.001 \text{ m}^2/\text{s}^3$.

For this case, a finer mesh than the coarse one developed for the thermal plume is introduced. The mesh in this case does not consist of uniform cells, they are smaller in the x,y direction along the centerline, in order to get a finer grid and capture in detail the expansion of the plume in these directions (Figure 5.2). The grid characteristics of the simulations, domain size L , number of cells N , average cell sizes Δ , time steps Δt and simulation time τ , are summarized in Table 5.1.

Table 5.1: Characteristics of the helium plume simulations.

Case	OpenFOAM grid	KFX grid
$L_x \times L_y \times L_z$ (m)	$4 \times 4 \times 16$	$6 \times 6 \times 14$
$N_x \times N_y \times N_z$	$96 \times 96 \times 240$	$125 \times 125 \times 131$
$\Delta_x \times \Delta_y \times \Delta_z$ (m)	$(4.1 \times 4.1 \times 6.6) \times 10^{-2}$	$(4.8 \times 4.8 \times 10.6) \times 10^{-2}$
Δt (s)	2×10^{-3}	5×10^{-3}
τ (s)	20	20

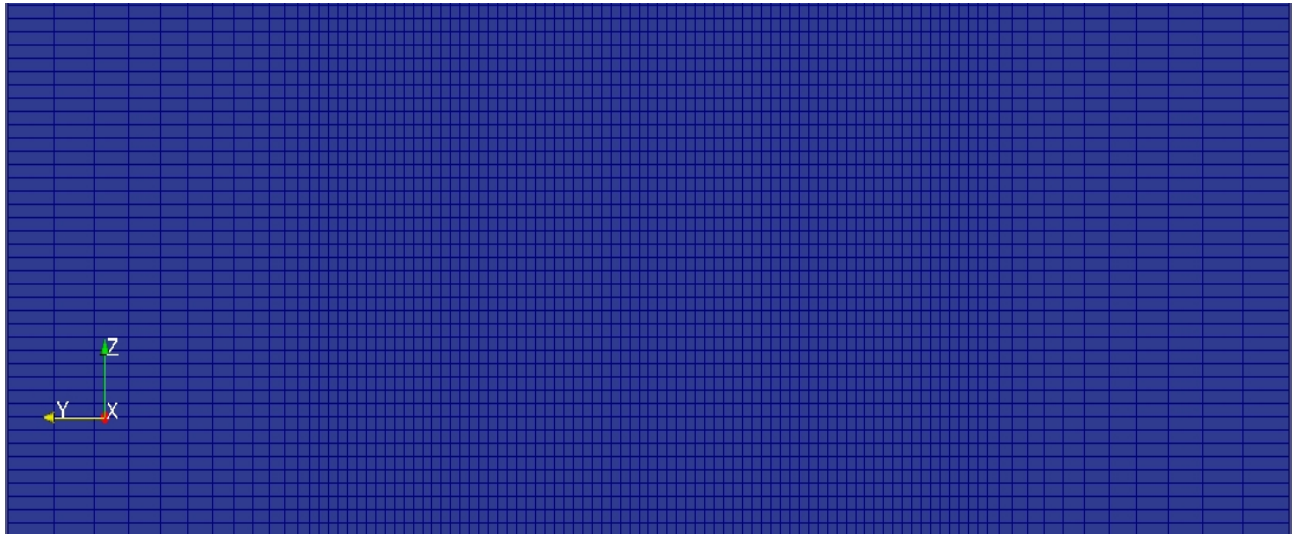


Figure 5.2: Representation of the domain across z direction. Cells are horizontally rectangular near the walls, and become denser and vertically rectangular closer to the centerline.

5.2 Simulation with OpenFOAM®

The OpenFOAM base directory file has a structure similar to the one presented for the thermal plume in section 4.2. Again, the files "0", "constant", "system" are present, containing the libraries that control the conditions of the experiment as discussed before.

5.2.1 OpenFOAM solver

The solver in this case is summoned with "rhoReactingBuoyantFoam", which is a solver optimized in combustions with chemical reactions, supported by a density based thermodynamics package and enhanced buoyancy treatment. It also uses a PIMPLE loop for pressure and velocity as the solver used for the thermal plume case.

5.2.2 Turbulence model

The turbulence model denoted "*dynamicKEq*" is again tested in this case, representing the dynamic one-equation eddy viscosity SGS model of section 3.3.1. The spatial filtering of the Navier-Stokes equations is utilized to describe buoyancy-driven flows, capturing the complex turbulence characteristics.

5.2.3 Boundary conditions

The "turbulentInlet" function for the velocity is reapplied here, inserting random fluctuations of the velocity in x, y, z directions as a fraction of the mean value. The function is already demonstrated in section 4.2.3. Fluctuation scale is set at 0.5 in x, y, z directions, while the reference field is 0.325 m/s in the z direction. The remaining boundary conditions are again considered as thermally and dynamically passive flow conditions.

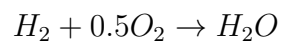
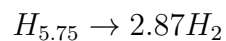
5.3 Simulation with KFX®

The KFX simulation was conducted by reconstructing the helium plume case according to Tieszen (2005), which has already been validated by ComputIT AS. The design of the geometry using Doozer interface provides a close representation of the experimental setup (Figure 5.3), using the characteristics for the simulation as demonstrated in Table 5.1. The current design does not include the original plan for the air inlet around the helium inlet source.

The grid nodes are denser in the x,y directions from the center, where they have the maximum density along the centerline. The domain and boundary records are inserted according to the ones specified in section 5.1.

5.3.1 Parameter setup

The composite fuel formula for the inlet is $H_{5.75}$ and the following reactions take place:



The discretization methods for the transport equations based on Gaussian elimination algorithms are implemented here, similarly with the thermal plume case. The time step is set to 5×10^{-3} , while the width of the temporal filter of the Navier-Stokes equations is set to 0.02 seconds. The eddies with larger time scale than this value are resolved with the TFNS

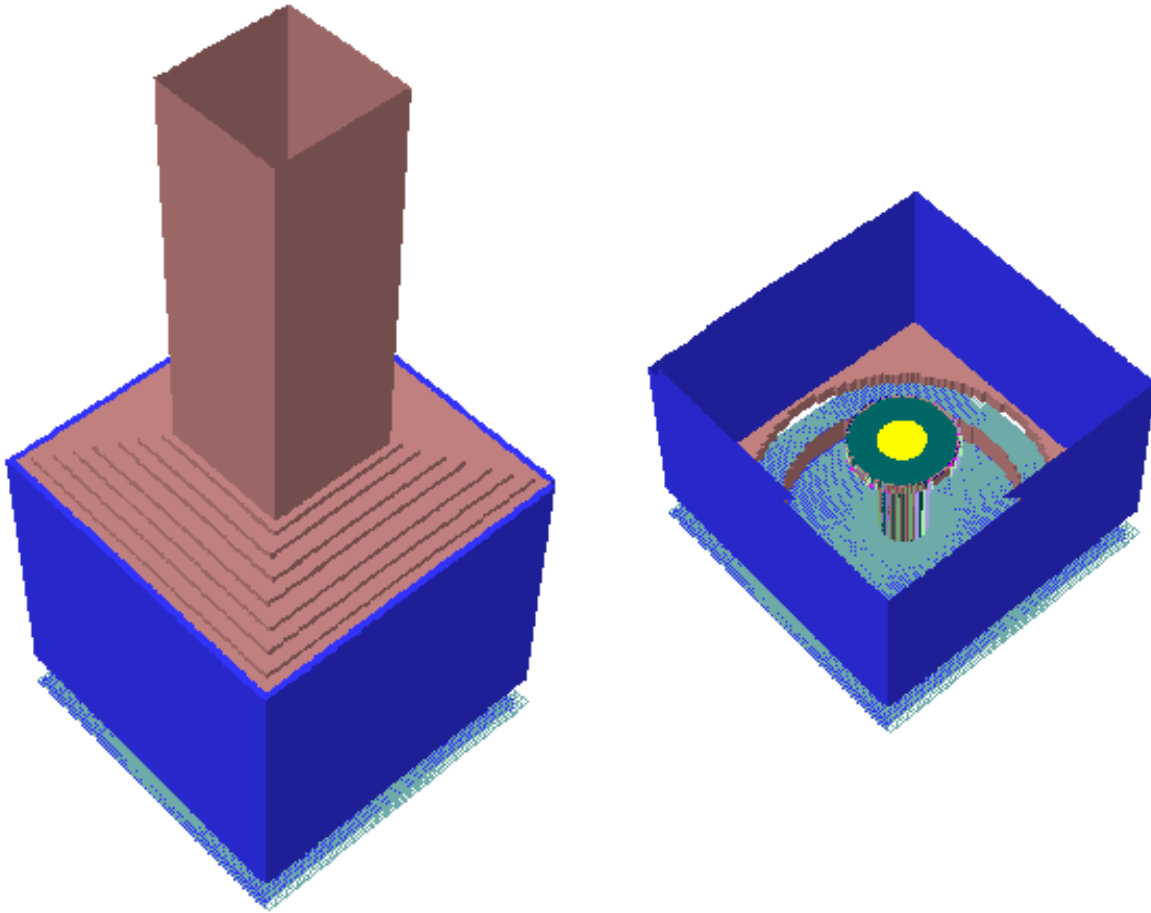


Figure 5.3: Geometry of the helium case in KFX from an external view (L) and without the chimney (R).

equations, while the ones with smaller are modelled. Noise amplitude in the inlet is not present in this case, so the injection has a constant rate of 0.325 in the z direction.

5.4 Results

Numerical results from the helium plume simulations are compared to the experimental data available from Tieszen (2005). The geometry in OpenFOAM is simplified into not containing the air inlet and the elevation of the source from the ground in OpenFOAM, while in KFX there are two different cases constructed, one similar to the experimental setup of Tieszen (2005) and one without the air inlet around the helium source.

As for the helium plume only velocity measurements are available, the extracted results are only for the centerline axial velocity. Quasi-steady state is assumed at 10 seconds, and the results are time-averaged for the interval of 10 to 20 seconds. Similarly to the thermal plume case, the numerical data from the most accurate simulation efforts are placed in the same figures with the experimental data.

The surface representation of the velocity from the KFX simulation at 20 seconds is demonstrated in Figure 5.4. In Figures 5.5 and 5.6, snapshots of the axial velocity magnitude are illustrated, at 20 seconds simulation time in OpenFOAM and KFX, respectively.

In Figure 5.7, the centerline averaged axial velocity (m/s) from all cases is compared to the experimental data available, against the distance from the source (z/D). Additionally, the data from the original simulation conducted by ComputIT AS are included here. The diameter of the helium source D has length of 1 m, and since the experimental data are collected close to the source, the figure represents the results up to the height of $4D$. Temperature data are not relevant for this case since the helium gas is in ambient temperature.

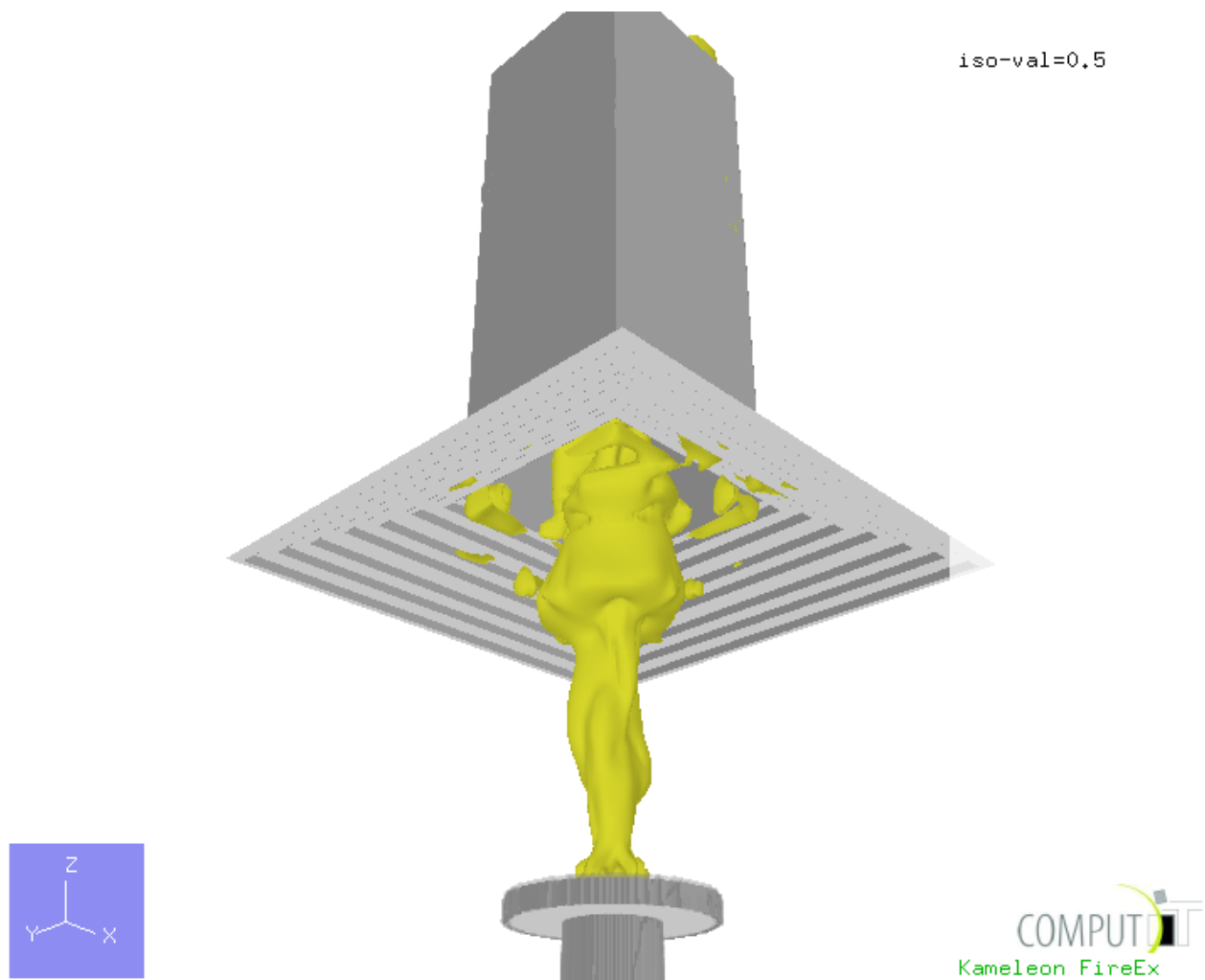


Figure 5.4: Development of the helium plume at 20 seconds with iso-surface value of 0.5. The puffing effect described in the start of this chapter is present.

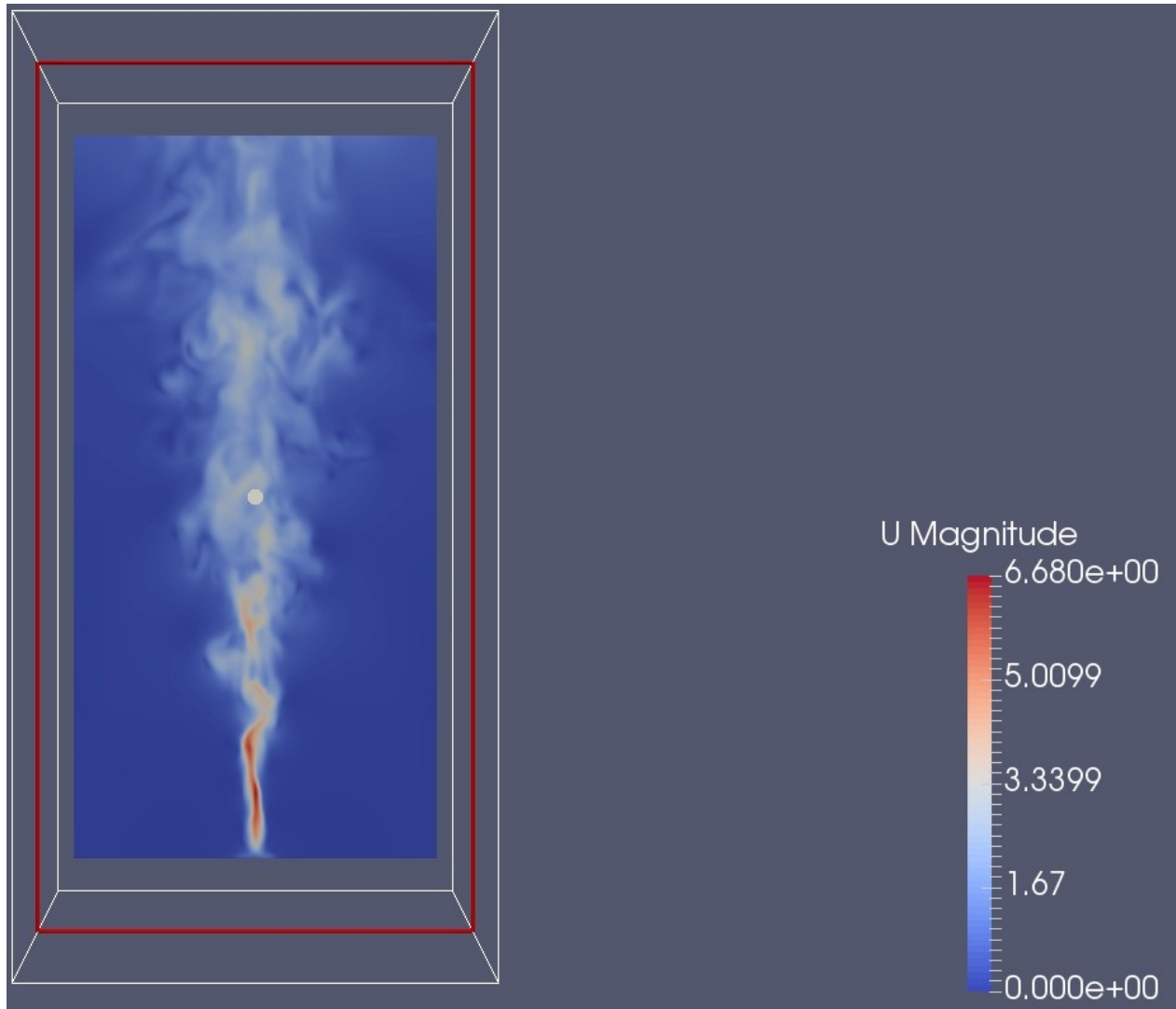


Figure 5.5: Snapshot of the axial velocity magnitude taken on a slice of the domain at the center of the geometry in OpenFOAM, at 20 seconds simulation time.

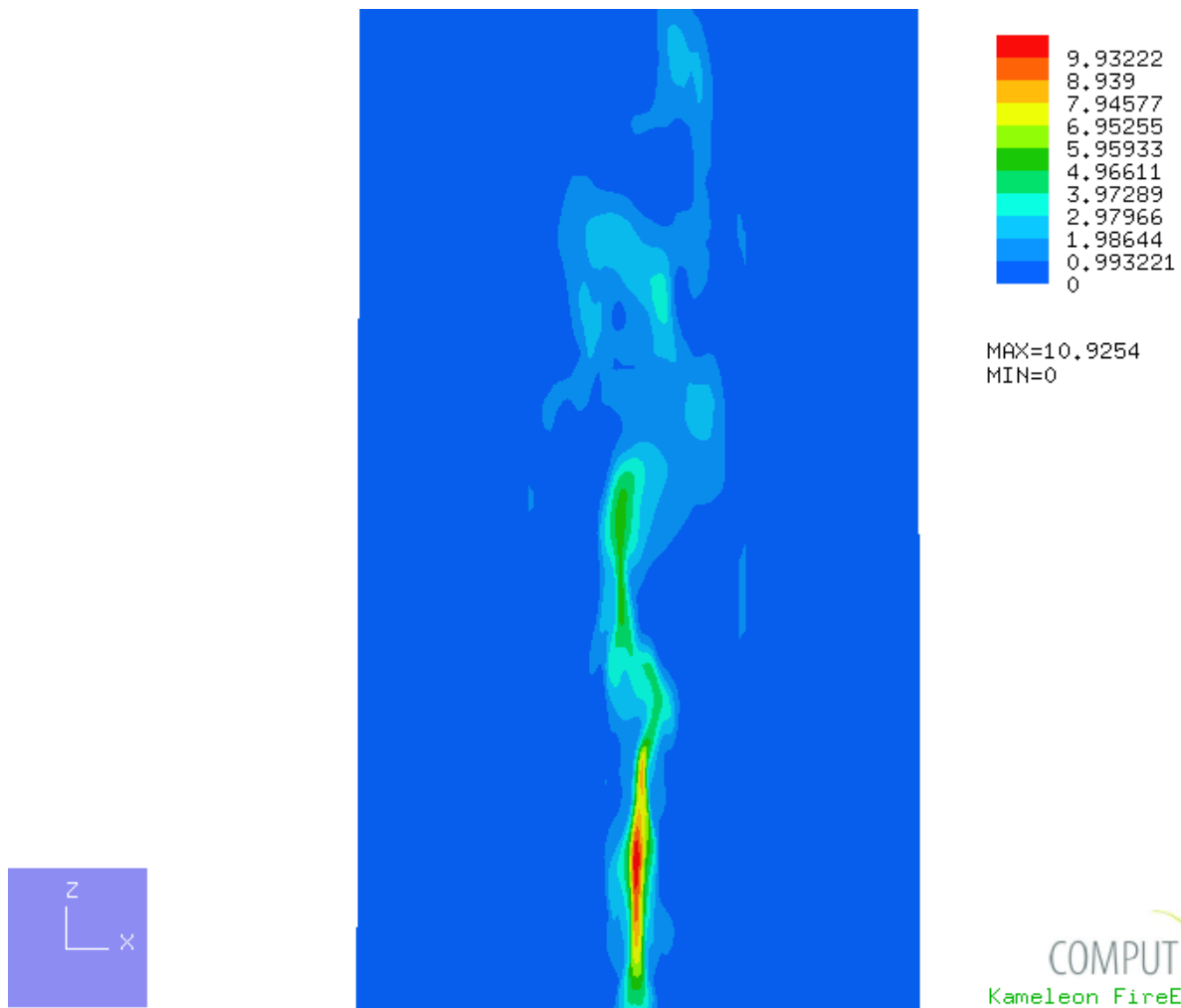


Figure 5.6: Snapshot of the axial velocity magnitude taken on a slice of the domain at the center of the geometry in KFX, at 20 seconds simulation time.

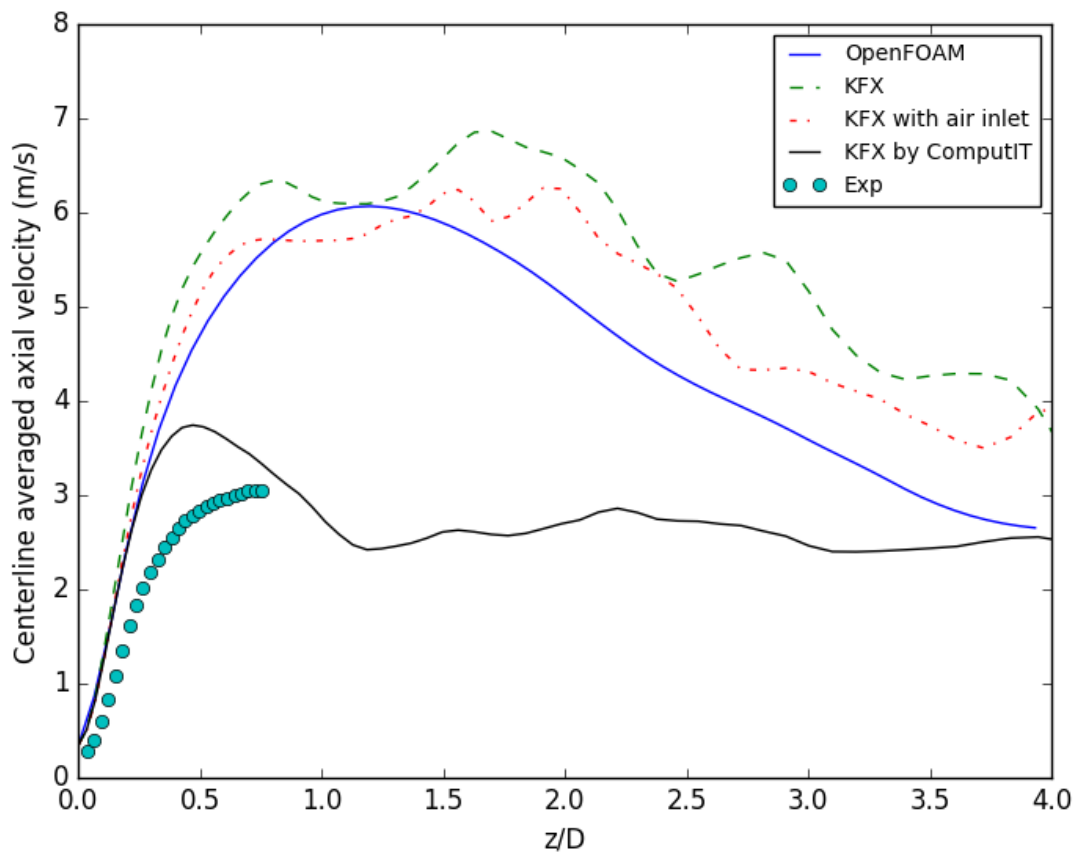


Figure 5.7: Centerline averaged axial velocity against the distance from the source for the helium plume ($\tau = 20$ s).

Chapter 6

CO₂ Plume

In this chapter, the focus is on simulating high-pressure liquid CO₂ releases from pipeline ruptures in Carbon Capture and Storage (CCS) facilities. There has been a lot of research and tests on the matter as it is shown in Chapter 2, since it is believed that burying CO₂ in CCS facilities is an effective way to tackle CO₂ emissions. However, a possible failure in these operations may result in severe consequences in the surroundings, and that is demonstrated through simulating such accidents. Although CO₂ is not flammable or explosive, during its phase transfer cryogenic conditions take place, and since it is heavier than air, risk of asphyxiation is present.

A presentation of the relevant literature and recent tests with other software apart from KFX has already taken place in Chapter 2. Experimental data from such tests are not yet publicly available, however, for the needs of this project, a "blind" test case is set up in KFX accordingly to COSHER experiment, that was conducted by Total E&P Norge.

6.1 Computational Setup

The case that is set up for this project is based on Total's COSHER experiment. In this experiment, a 94.08 m pipe with a diameter of 8" is buried 0.5 m below the ground. The rupture section is in the middle of the pipe, while the storage pressure is at 150 barg with ambient temperature of 300 K. The experimental structure is demonstrated in detail in Figure 6.1.

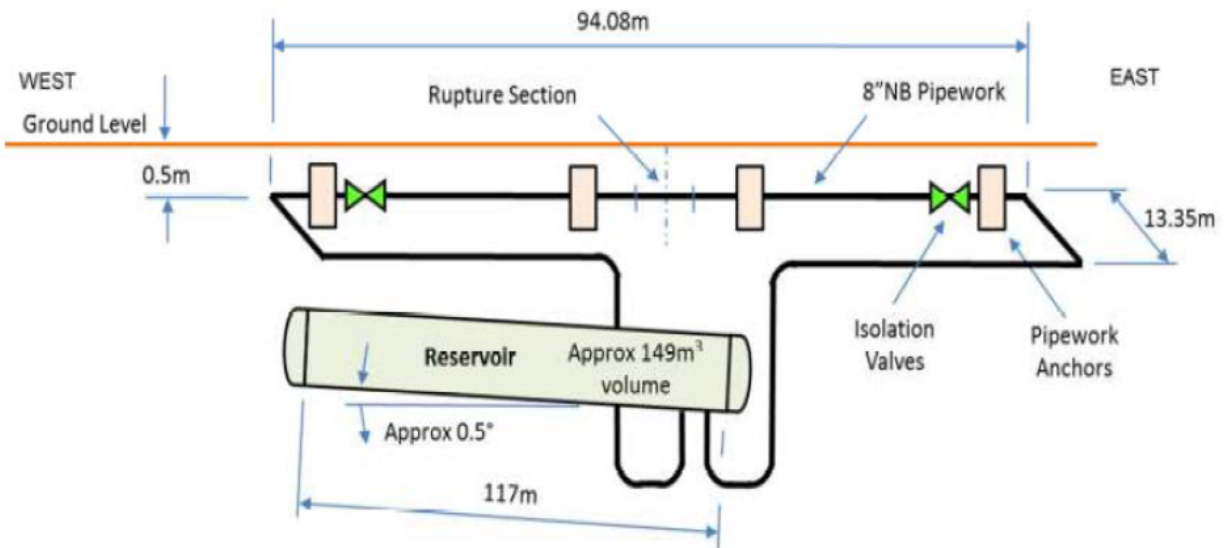


Figure 6.1: COSHER experiment structure (figure from Total E&P Norge presentation by Pacaud, F and Tonda, H during KFX user meeting in Trondheim, Norway (2014).)

CO₂ is maintained with high pressure in liquid form during the pipeline transport, where a rupture may occur. Such incident will result in immediate transformation from liquid to gas, due to the drop of pressure to atmospheric. An instantaneous multiphase expansion is observed along the vertical axis, with a significant drop in the ambient temperature and solid particle formation that disperse and sublimate. Closely after, due to the fact that CO₂ is much heavier than air, the expansion will continue towards the ground surface. It can be considered as the opposite phenomenon of the helium case (helium is much lighter than air), and grows many concerns as a large area may be affected from such release.

The complexity of the phenomenon and the sub-processes that take place require advanced simulation tools and functions which, to the author's knowledge, are not yet publicly available with OpenFOAM. Thus, this case is set up only in KFX, where CO₂ releases have already been validated by ComputIT AS in tests performed from oil companies Shell and BP (section 2.3). Images from aerial views during the COSHER experiment are displayed in Figure 6.2.

The domain of this case covers a much larger area than the other experiments, since the dimensions here are bigger (pipeline length of 96 m). With the rupture placed in the center, the domain expands to 1600 m in the x direction and 800 m in the y, z directions. This is

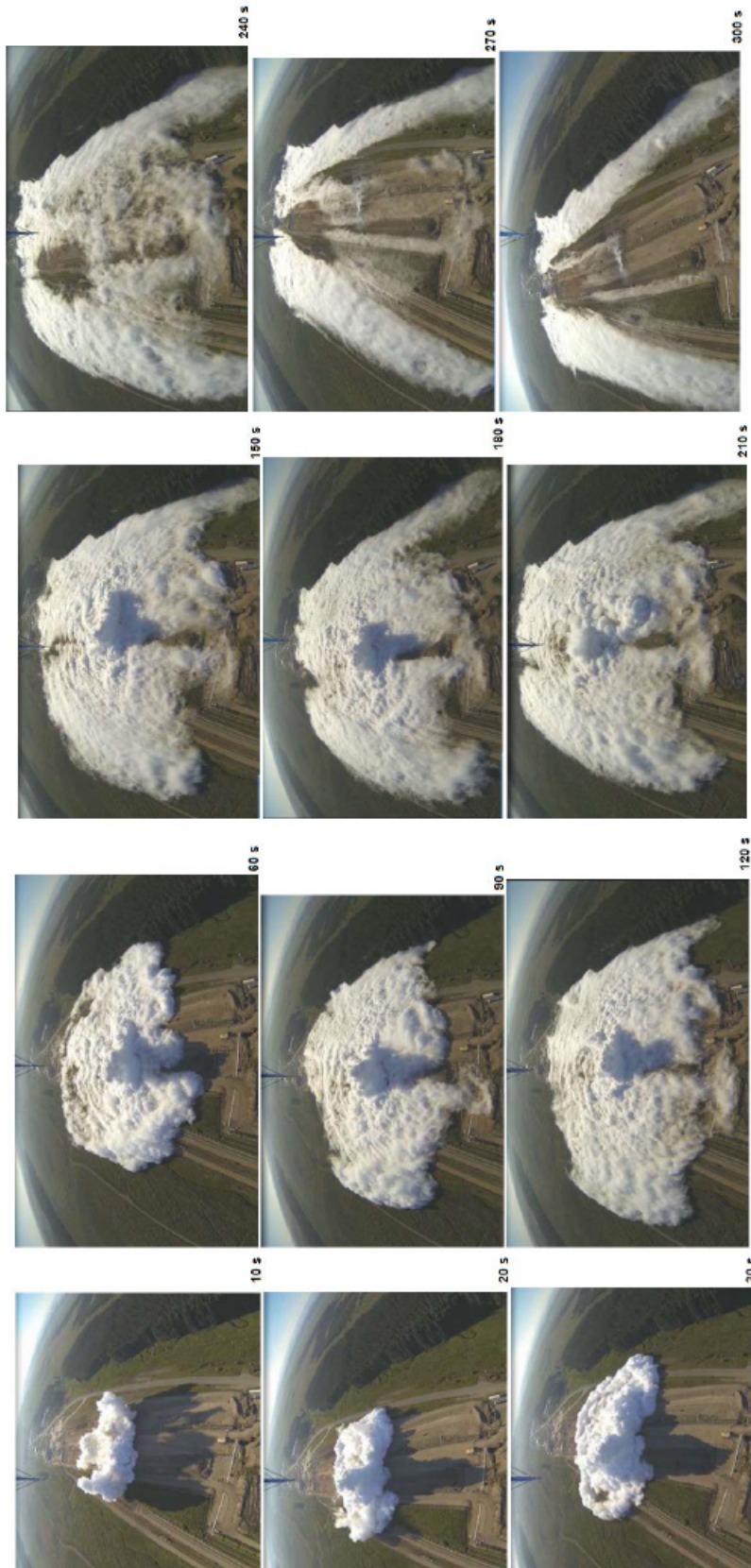


Figure 6.2: Aerial view of the COSHER experiment during 300 seconds after the release (figure adapted from Total E&P Norge presentation by Pacaud, F and Tonda, H during KFX user meeting in Trondheim, Norway (2014).)

because atmospheric wind conditions are present with a logarithmic velocity profile in the x direction, so the expansion will mainly take place towards it. The mesh is composed of 202 cells in x direction and 102 in the y,z , resulting in a total of 2101510 grid nodes. The grid nodes are concentrating near the center and are more spacious on the edges of the domain. Ambient temperature and pressure are stable at 300 K and 101325 Pa respectively, while turbulence parameters k and ϵ are set to $1 \text{ m}^2/\text{s}^2$ and $10 \text{ m}^2/\text{s}^3$.

KFX includes an expanded jet calculator tool which, given the reservoir pressure (150 barg), source diameter (0.2 m), the ratio of specific heats (1.3) and the molecular weight of CO₂ (44 kg/kmol) calculates the outflow gas velocity at 445.5 m/s. This calculator assumes all the momentum to be forced in the vertical direction, but since the rupture is in the middle of the pipeline, momentum gets significantly reduced as it is distributed in all directions. Therefore, the outflow gas velocity is assumed at 100 m/s and the mass flow rate is reduced accordingly. A low temperature of 100 K is also assumed for the CO₂ inlet, to account for the heat extracted from the surroundings with the transition of liquid to gas, following the change from high to atmospheric pressure, as it is described analytically in section 2.1.

The grid characteristics of the simulations, domain size L , number of cells N , average cell sizes Δ , time steps Δt and simulation time τ , are summarized in the table below. The grid should be quite more dense in normal conditions, but due to the high requirements in computational times, a simplified format is applied here.

Table 6.1: Characteristics of the CO₂ plume simulation.

Case	KFX grid
$L_x \times L_y \times L_z$ (m)	$1600 \times 800 \times 800$
$N_x \times N_y \times N_z$	$202 \times 102 \times 102$
$\Delta_x \times \Delta_y \times \Delta_z$ (m)	$7.92 \times 7.84 \times 7.84$
Δt (s)	2×10^{-3}
τ (s)	30

6.2 Simulation with KFX®

The geometry is designed with KFX doozer tool, with the assumption that the pipeline is not buried beneath the surface but is placed on top. A uniform grid is utilized here, and the domain and boundary records are set similarly to the ones specified in section 6.1.

Two different wind profiles are tested to mimic the experimental conditions. A logarithmic wind profile is introduced, with a velocity of 5 m/s towards the x direction 10 m above the surface for the first and 10 m/s for the second test. The wind in this velocities is regarded as a gentle breeze and as a fresh breeze, respectively (Windfinder, 2017).

6.2.1 Parameter setup

The injected gas is 100% composed of CO₂ and the temporal filter of the TFNS equations is set to 0.5 seconds, due to the larger scale of this experiment compared to the previous ones. Since a detailed description of the COSHER experiments is not available, various choices were tested to evaluate the effects. Simulation time of 30 seconds is considered enough to capture the phenomenon in a small scale. As mentioned in section 6.1, outflow velocity of 100 m/s and temperature of the mixture at 100 K are specified.

6.3 Results

The CO₂ release is represented by displaying the concentration profile along the distance from the crater, towards the wind velocity. An indicative surface presentation of the CO₂ concentrations from the release point to some meters along the wind direction is illustrated in Figure 6.3. These results are extracted for the gentle wind conditions.

The concentration profile of the CO₂ plume along the distance from the crater up to 200 meters to the wind direction is presented in Figure 6.4. The vertical axis represents the volumetric concentration (percentage) while the distance to the crater (m) is represented in the horizontal axis. A logarithmic profile is used for the wind velocity, which is adjusted to 5 m/s towards the x direction to represent a gentle breeze, and to 10 m/s to represent a fresh breeze (Windfinder, 2017).

In Figure 6.5, a closer view on the results is presented for lower concentration values and starting from 50 meters away from the crater. It is noticeable that in fresh wind conditions, CO₂ concentrations may be detected up to 350 meters away from the source, 30 seconds after the release.

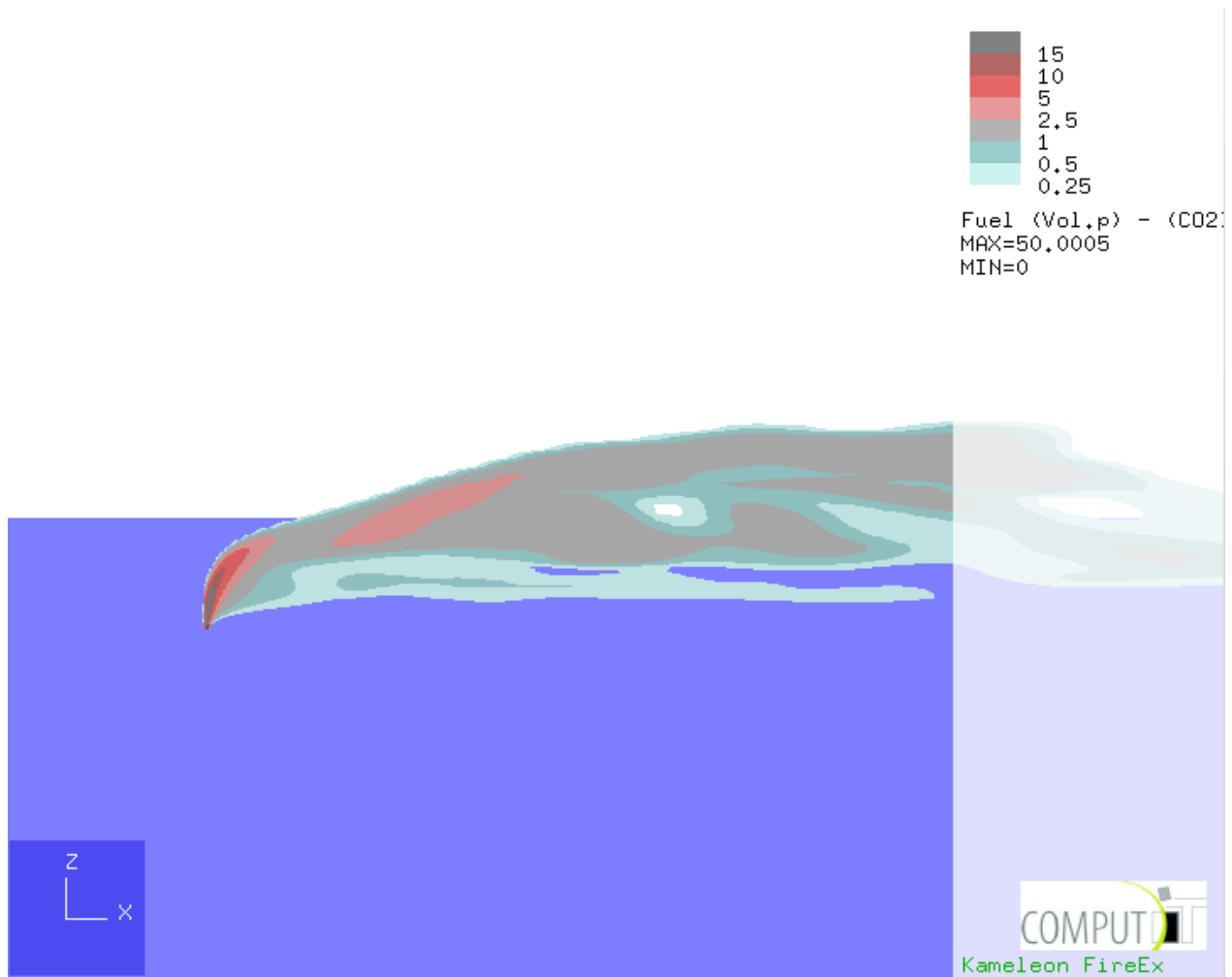


Figure 6.3: Surface presentation of the CO₂ concentrations 30 seconds after the release, along the wind direction.

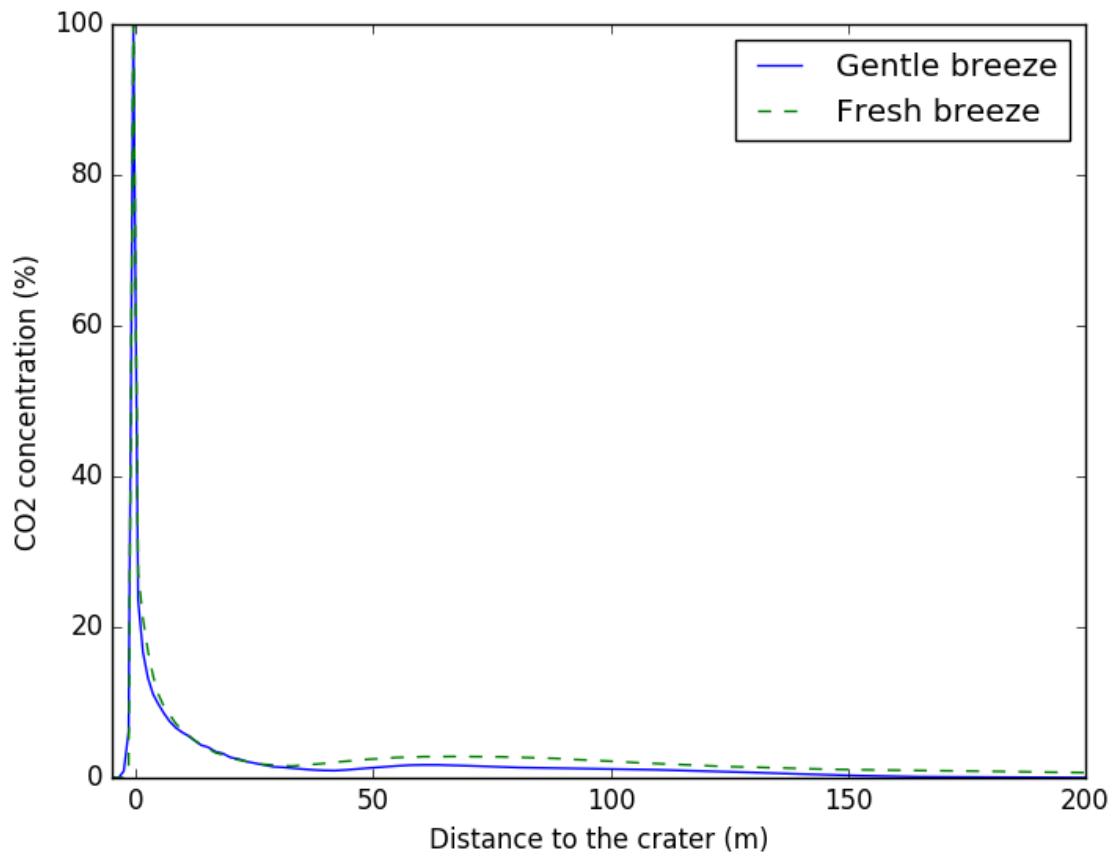


Figure 6.4: CO₂ concentrations downstream of the crater towards the wind direction at 30 seconds, for gentle and fresh wind conditions.

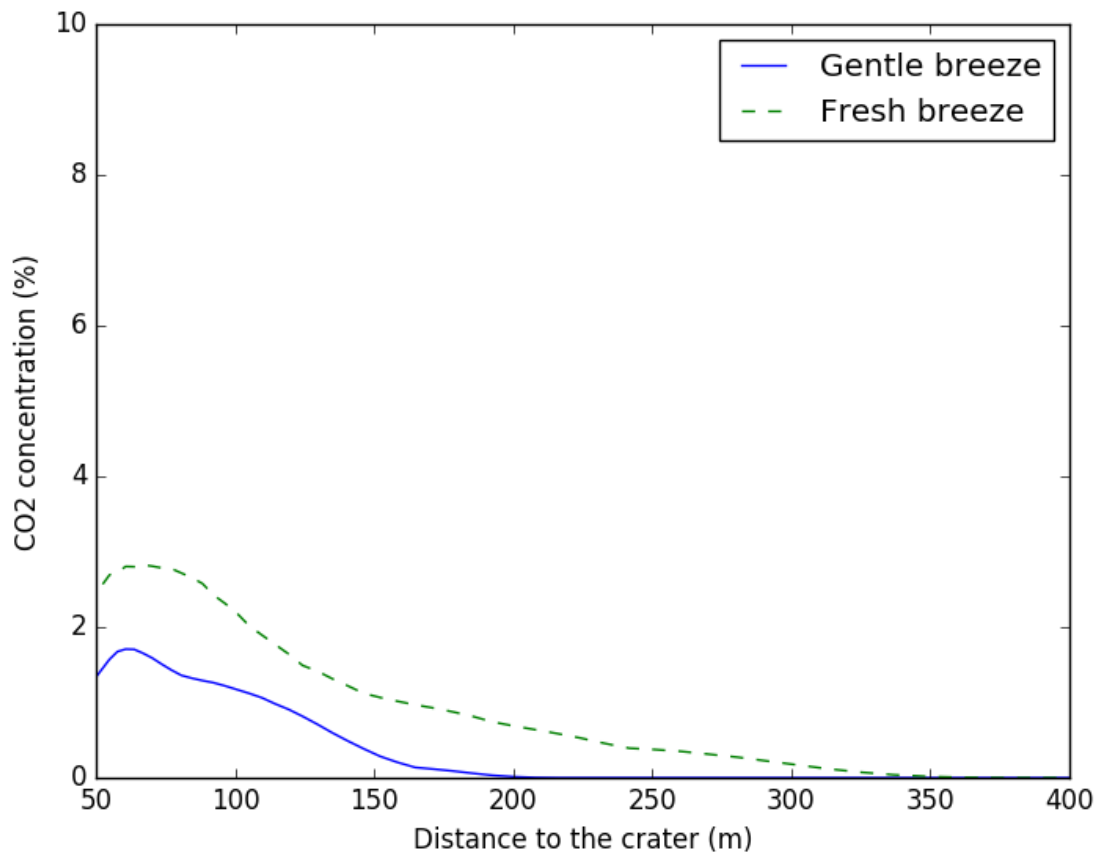


Figure 6.5: CO₂ concentrations from 50 meters downstream of the crater towards the wind direction at 30 seconds, for gentle and fresh wind conditions.

Chapter 7

Discussion

Direct comparison between numerical and experimental data helps validating the correct implementation of the turbulence model and identify the weaknesses that need to be highlighted. For the first two cases that experimental data is available, it is clear that there are a few challenges to be tackled with the LES model implementation. These challenges include the generation of turbulence close to the inlet source, and the construction of a grid that accurately resolves the dispersion without exceeding the computational time limitations. Furthermore, an important issue in CFD simulations is specifying a proper writing interval for storing results. An averaging in the same time interval but with fewer data may yield different and more inaccurate numerical results.

7.1 Fluctuations in the inlet

The insertion of random fluctuations as function of the average flow in OpenFOAM (accordingly to Equation 4.1) is a way to overcome the delay in turbulence generation, and works well for the thermal plume case, as it can be deduced from the results (Figures 4.7, 4.8). However, these fluctuations are introduced randomly, therefore they do not necessarily make physical sense. Furthermore, in order to reach these results, a fluctuation scale of 0.5 was used, which is considered quite large. KFX software, which does not have such a function, overpredicted the results for the thermal plume case. The turbulence generation starts away from the inlet source so the dispersion of the gas is not decelerated enough by

it. Without the noise insertion in the inlet, both the TFNS model of KFX and the DOEEV model of OpenFOAM overpredict the results, as it will be shown later on (Figure 7.5).

Judging the results in Figure 5.7, these fluctuations in the inlet do not seem to be enough for the helium plume though, where buoyancy depends on the density rather than the temperature difference. Here, that both simulations overpredict the experimental data, and the KFX model actually works better for this case as similar results are reached without the noise amplitude in the inlet source. In this case, the fluctuation scale of 0.5 which was again used in OpenFOAM, was not enough to slow up the dispersion of the helium gas, which had almost double velocity values compared to the experimental ones (Figure 5.7). The increase of the fluctuation scale closes the distance between experimental and numerical values (Figure 7.1), but cannot be explained physically and the simulation loses its realistic character.

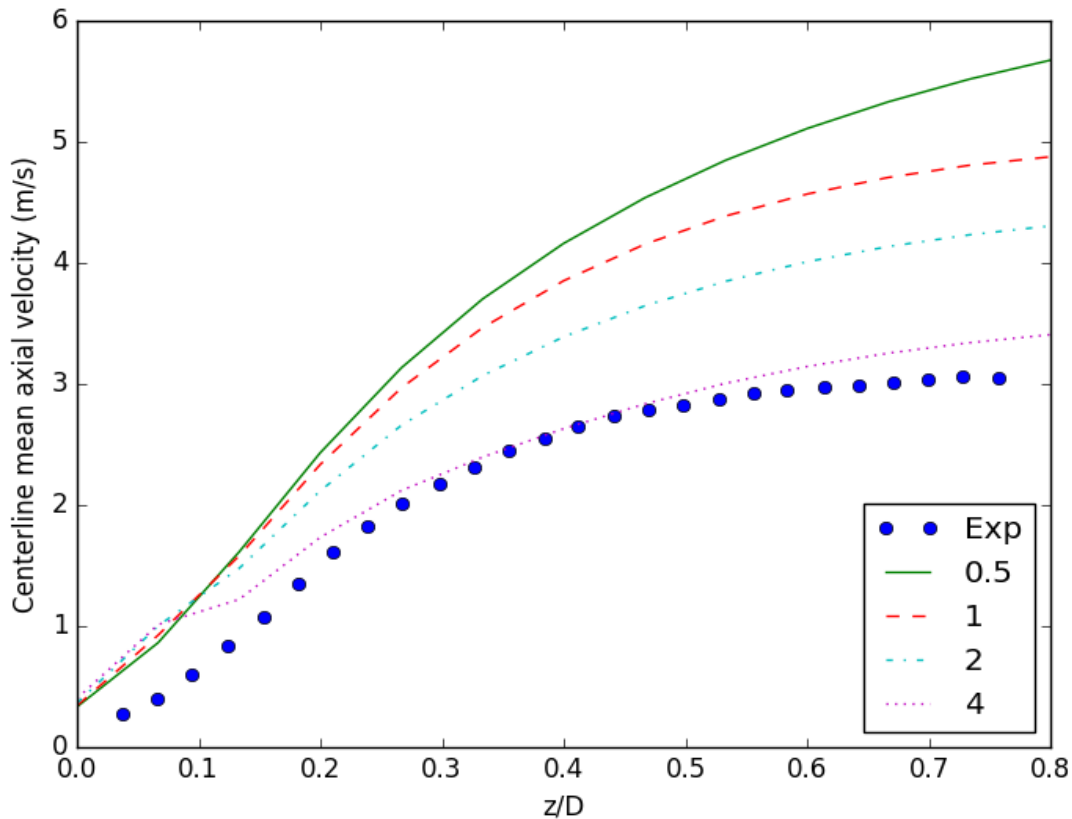


Figure 7.1: OpenFOAM results for the helium case, for fluctuation scales in the inlet of value 0.5, 1, 2 and 4.

The CO₂ plume that is simulated only with KFX does not utilize any fluctuation scales in the inlet, but even if such function was available it would not be needed in this case. The jet release itself establishes the turbulence field automatically due to the much higher density of CO₂ than air, and the diversity in the directions of the dispersion.

7.2 Grid scales

The mesh and grid node sizes and distributions are parameters that directly affect the simulation process. Due to the higher time requirements of detailed grids and the time constraints for the submission of this project, the number of grid nodes is set to an approximate low level for each case.

The coarse grid of the thermal plume case consists of $46 \times 46 \times 123 = 260268$ grid nodes. For this particular case though, this number of grid nodes is considered enough as results are satisfying and only slightly less accurate than the fine grid, which utilizes $92 \times 92 \times 246 = 2082144$ grid nodes. This can be deduced from Figures 7.2, 7.3, where the results between the two grids and the experimental data are compared for the centerline averaged axial velocity and temperature.

Judging from the region that the experimental data are collected, it is safe to suggest that there is no need to further increase the grid node number for this case. Between the two, the coarse grid is the optimal solution as the computational cost is significantly reduced.

In KFX, a number of $51 \times 51 \times 130 = 338130$ nodes is used, and even though that value is larger than the OpenFOAM case, results deviate more. The challenge is located in enforcing the turbulence near the source without the use of random inlet fluctuations, and this is independent of the grid size.

The grid scale has more importance when simulating the helium and CO₂ plumes. Concerning the helium case, in OpenFOAM $96 \times 96 \times 240 = 2211840$ grid nodes are used, and in KFX $125 \times 125 \times 131 = 2046875$ grid nodes, with the difference that the nodes in OpenFOAM are more quadratic and in KFX more rectangular and concentrated near the source. However, these numbers are far from the ones used in the setup of Tieszen (2005), where

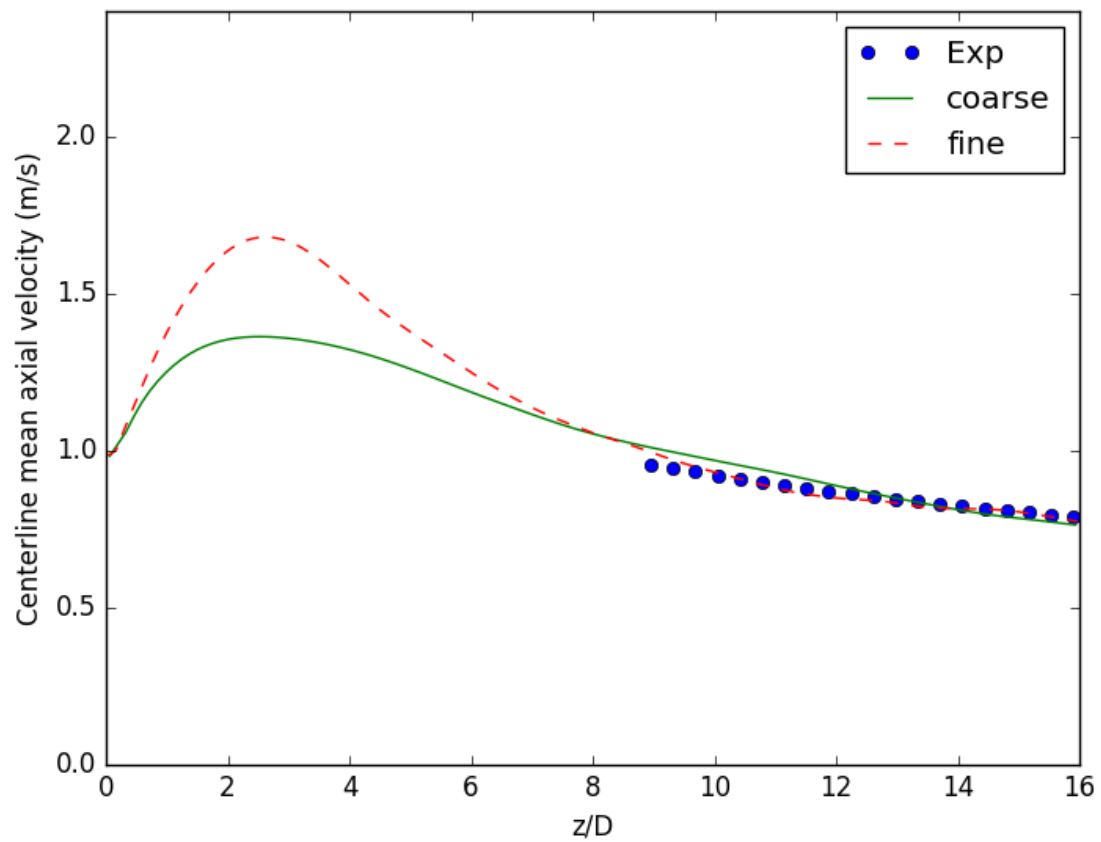


Figure 7.2: Centerline axial velocity results between the coarse and the fine grid for the thermal plume in OpenFOAM, $\tau = 30$ s.

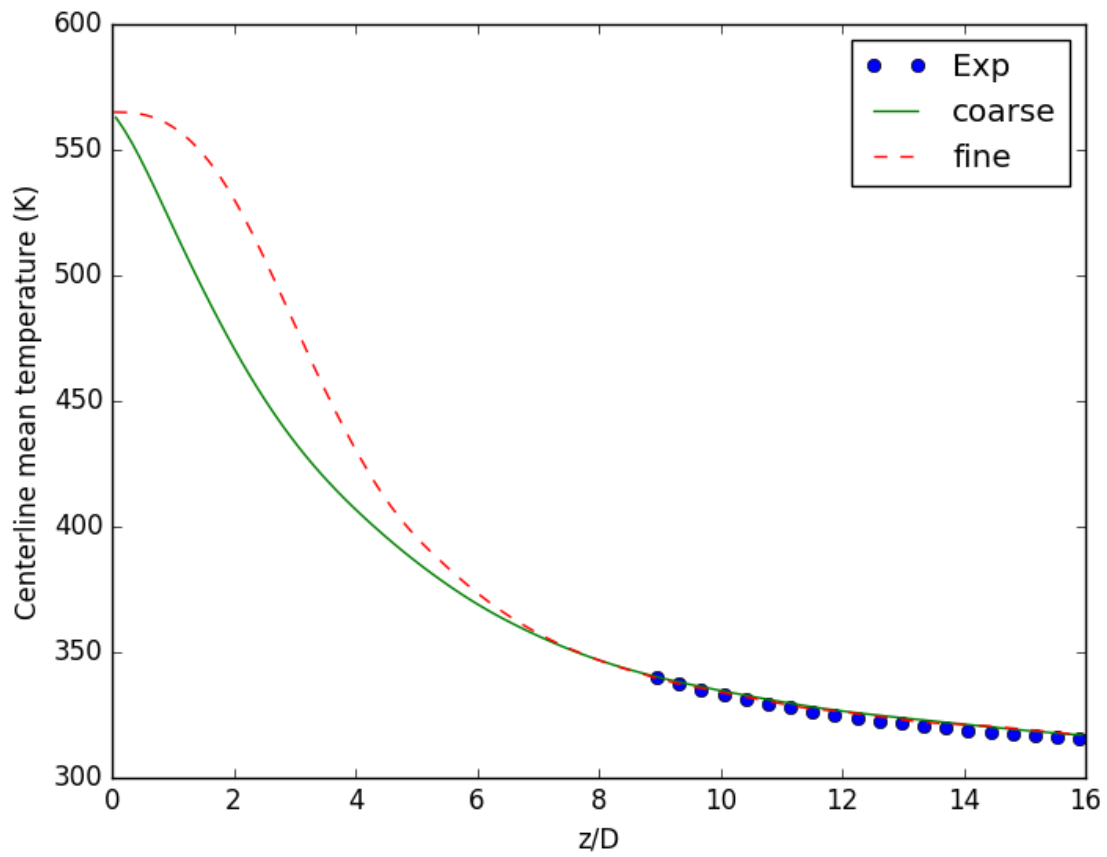


Figure 7.3: Temperature results between the coarse and the fine grid for the thermal plume in OpenFOAM, $\tau = 30$ s.

approximately 10 million nodes are utilized (5 times larger number of nodes). This is an important reason for the deviation of the simulations to the experimental data in this case, especially for the ones performed in KFX. Since results are identical in both OpenFOAM and KFX, the KFX simulations are considered more successful as no function for fluctuations in the inlet source is used and the turbulence is generated only from the TFNS model.

The CO₂ grid consists of $202 \times 102 \times 102 = 2101608$ grid nodes, with a concentrated distribution in the center of the domain where the release is located. Since the nodes have an average dimension of approximately 8 meters to all directions, it is important to shorten the ones near the source to effectively describe the multiphase expansion, as the solvers are applied in smaller blocks. The grid nodes which are placed closer to the edges of the domain are of less computational importance since they are located away from the bulk of the flow.

7.3 Data writing intervals

A significant feature when processing simulation results is the number of individual data that are collected, the writing interval in which data are saved. The smaller the writing interval, the more data are stored and are available in the time-averaging process when the quasi-steady state is assumed. The importance of that is highlighted in the helium plume case, where analytical results for every 0.05 seconds for a total simulation time of 90 seconds are collected by ComputIT AS during the company's process of validating the helium plume simulation. Within the frames of this project, such amount of data are unable to handle due to time and disk space limitations and data are stored for writing intervals of 1 second.

However, to obtain an insight to that, the time-averaging process is applied to the axial velocity data of the helium plume for the time interval of 10 to 20 seconds. In that same time interval, results are collected every 1 second and every 0.25 seconds. The results between the different writing intervals are displayed in Figure 7.4. The curve produced by the time-averaged results that are produced every 0.25 seconds is visibly smoother and closer to the experimental data. If the writing interval is even smaller, and for a larger

time-averaging interval as the one used by ComputIT (90 seconds), numerical results are expected to be even more satisfying, closely matching the experimental data.

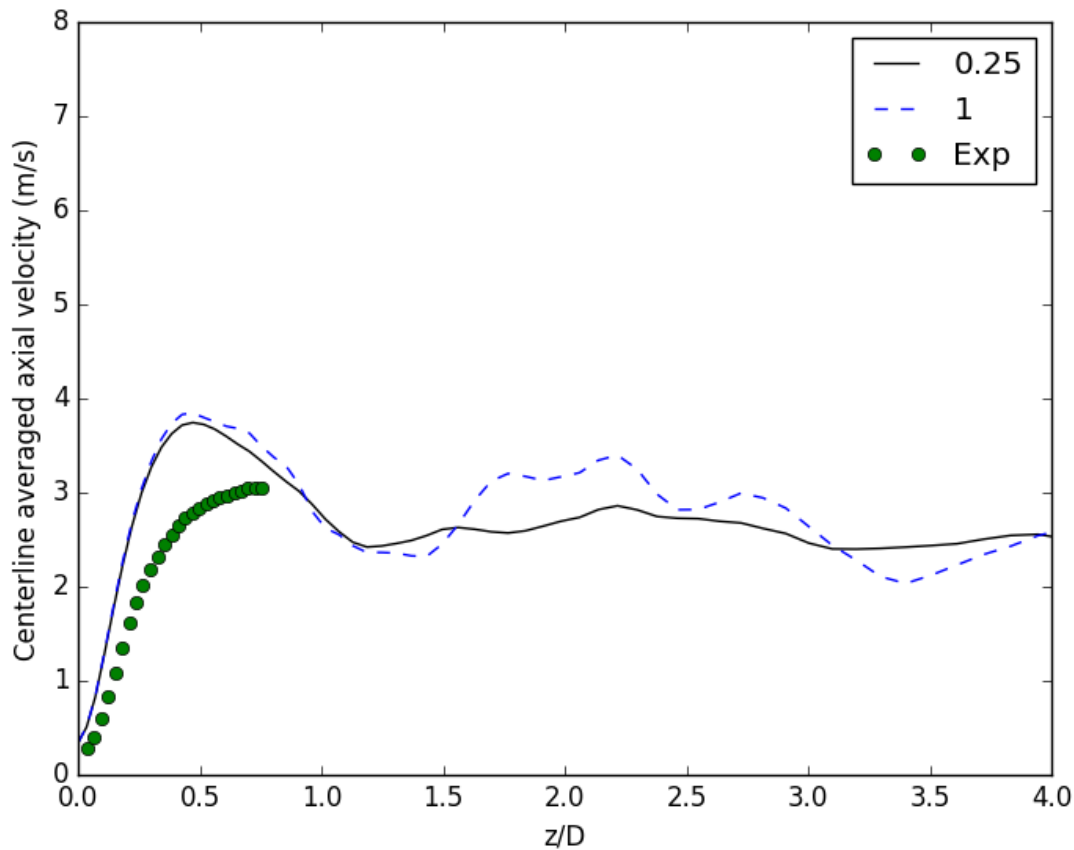


Figure 7.4: KFX results for the helium plume, with a data writing interval of 0.25 and of 1 second.

The challenge of time-averaging the data is alleviated in OpenFOAM, where an averaging function that runs while the simulation runs is available, denoted 'fieldAverage'. A recommendation for all CFD software would be to have such function implemented as well.

7.4 LES model

The characteristic difference between the DOEEV model of OpenFOAM and the TFNS model of KFX, is that the first is based on spatial filtering while the second is based on temporal filtering. Judging from the computational times of the simulation processes, temporal

filtering enhances more the speed of the simulation than the spatial one, and adjusting the TFNS filter width in higher values resolves the eddies with even larger time scales while the ones with smaller are modelled. The question that needs to be answered is "how much loss of simulation accuracy is accompanied with that?".

Considering the thermal plume case, it is not representative in answering this question, as the problem with the turbulence generation in the KFX simulations is located in the absence of the random fluctuations in the inlet. Without the use of the relevant function in OpenFOAM, numerical results from both softwares are deviating from the experimental data (Figure 7.5).

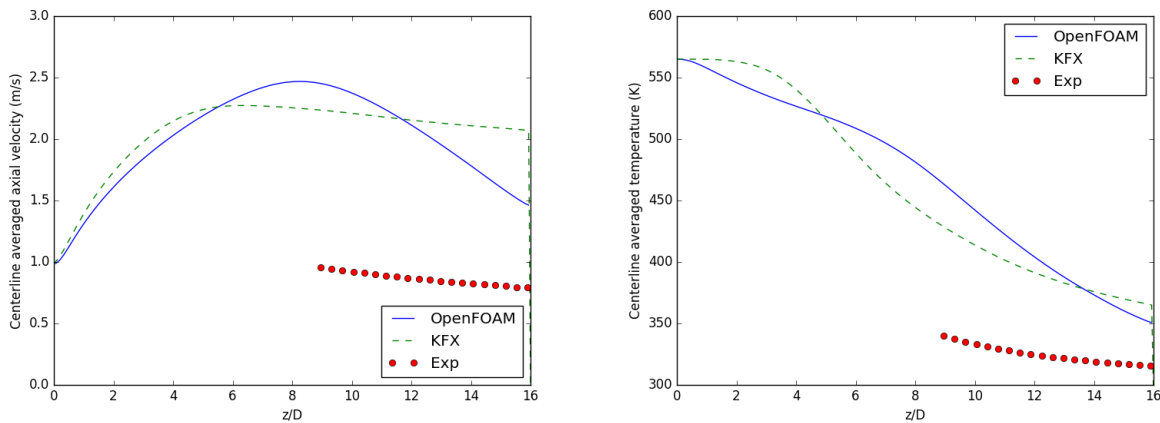


Figure 7.5: Centerline averaged axial velocity (L) and temperature (R) data for the thermal plume, without the insertion of random fluctuations in the inlet in OpenFOAM ($\tau = 30$ s)(indicative sketching).

Regarding the helium plume, a relatively small filter width is used in the TFNS model (0.02 seconds), to capture the more detailed turbulence generation than the thermal plume. The time step used in KFX is larger than the one in OpenFOAM (Table 5.1), meaning that less computational resources are utilized in the process. In terms of computational times of the thermal and helium plume simulations, it would not be accurate to directly compare the two software. For the OpenFOAM simulations the university's server "gorina" is utilized, with varying permissions to computational resources inversely proportional to the active users, so the number of CPUs that were used varied from 8 to 32. On the other hand, the KFX simulations run on a single CPU, thus the decomposition of the total process is not yet

available.

What matters most though, is that numerical results from both models show deviation from the experimental data. However, the importance of collecting a large number of data to be averaged has already been mentioned in section 7.3, and in addition to that, the helium plume has a greater dependency on the grid scales. Particularly for the implementation of the LES model though, an important characteristic of this plume known as the puffing effect (Chapter 5), is captured only in the KFX simulations (Figure 5.4).

For the CO₂ plume, the TFNS model has a filter value of 0.5 seconds, which is a reasonable value considering the scale of the domain. KFX solvers effectively capture the multiphase expansion, and the turbulence model qualitatively describes the actual event. As there are no experimental data available to compare, this case is supposed to give a strong insight on the consequences after a high pressure liquid CO₂ release from a rupture in pipelines of CCS facilities.

7.5 General remarks

Judging from the results obtained for each case, the following facts are inferred:

- The dispersion of the thermal plume is decelerated by the turbulence taking place close to the source, and this is the main characteristic to be captured when performing a CFD simulation of this phenomenon. Additionally, fluid temperature drops relatively fast after the injection, as much of the thermal energy is transported to eddies as kinetic energy.
- The turbulent kinetic energy spectrum is an approved way of validating the LES model implementation. In the thermal plume, it can be seen that the energy spectrum follows the expected decay in the inertial range, described by the $-5/3$ law (Equation 3.8), followed by the -3 slope as a result of the buoyancy effects.
- The same challenge (decelerating the gas dispersion by enforcing turbulence generation close to the source) is also faced in the helium plume, along with capturing the puffing phenomenon which is more intense here. Satisfying results are achieved

by KFX without the insertion of random fluctuations in the inlet, and a more detailed grid with smaller writing intervals for the time-averaged data should yield even better results.

- Regarding the CO₂ release, it is difficult to evaluate the accuracy of the simulation without comparison to experimental data. However, considering the validation that has already been conducted by ComputIT AS, it is important to notice that in a small interval of 30 seconds after the release, CO₂ concentrations can be felt up to 350 meters away from the crater depending on the wind conditions. Should a full scale simulation of 300 seconds with a slightly stronger wind profile is conducted, chances are that the CO₂ concentration would have an even higher value and for a larger distance to the crater.

As the numerical results from these simulations are intended to be of use when planning for safety, it is of vital importance to have an uncertainty margin to the data collected. The technical risk analysis process needs to account for possible deviations to real-life incidents, and additional barriers need to be considered.

Chapter 8

Conclusions

The principal objective of this report, testing the implementation of LES models into thermal, helium and CO₂ plume simulations is largely met. LES models can be thought as a compromise between RANS and DNS, meaning that they are able to deliver simulations with accuracy close to the one that is achieved by DNS, with a significant save in computational resources which is the main feature of RANS. This is the reason that they are thought as quite promising models in capturing the turbulence phenomenon in flows, and expectations are that they will be largely used in the future.

Despite the rather simple geometry of the analyzed cases, they have a high complexity level due to their unique mixing and entrainment characteristics. Those parameters have an important role in the turbulence production and evolution along the gas dispersion. From the thermal and helium plume cases, it can be deduced that the main challenge is capturing the phenomenon of turbulence close to the source, where kinetic energy is transported to the eddy formation so the overall dispersion has a decelerated rate in the simulations.

The main challenges faced when conducting such CFD simulations are identified during the experimentation with each test case. Insertion of random fluctuations in the inlet source, adjustment of the grid scale, selection of a proper data writing interval for the time-averaging of the results and validation of the correct implementation of the LES model are highlighted as the principal debated fields in the process.

8.1 Summing up

The degree of accomplishment for the objective stated in section 1.5 is evaluated here. The tasks that the objective is divided into are stated below, and the level of fulfillment is discussed.

1. Evaluating the turbulence model of each software in the test cases.

The first task is to test the implementation of the DOEEV model in OpenFOAM and the TFNS model in KFX. The parameters for DOEEV affect mostly near-wall modelling that is not relevant in the examined cases, while for TFNS an appropriate filter width must be chosen. After experimenting with diverse choices, width values have been suggested for each test case, by comparing the effects in the numerical results.

2. Setting up simulation parameters that provide satisfying results.

By consulting the relevant literature and experimenting with diverse parameters, specific values are suggested for each test case. Results are considered satisfying for all the cases, at least to the extent that these parameters are affecting the simulations.

3. Comparing the numerical results from the two software to experimental data.

Post-processing is conducted simultaneously for the results provided by both OpenFOAM and KFX, and the numerical results are directly compared to the experimental ones. This refers to the thermal and helium plume cases, where experimental data are available.

4. Identifying the challenges faced in the simulation processes.

This task is fulfilled in a good level, as the main challenges that have been faced during the simulation efforts are underlined. Additionally, techniques to encounter them are suggested.

8.2 Recommendations for future work

Beyond the frames of this project, by utilizing more computational resources and hard disk space, more detailed numerical results are able to be extracted for the thermal, helium and CO₂ plumes.

Since the data writing intervals have an important role in the time-averaging process, which directly affects the the numerical results, the implementation of an averaging function for the data during the simulation process is recommended. Higher grid resolutions also improve the quality of the simulation, but this must be balanced with the available computational resources. It should not be forgotten that higher resolutions are not always needed, as for the thermal plume results between the coarse and the fine grid have insignificant differences.

Especially for the CO₂ plume, having the capability to conduct a simulation capturing the whole time interval of the COSHER experiment (300 seconds) will provide even more realistic results and will increase the awareness in case of such incident. Ideally, the grid resolution and domain size could be increased also as the full expansion is expected to cover a fairly large area.

The focus is suggested to be given in further validating the LES models, along with further experimenting with their adjusted parameters. High temporal filter widths for the TFNS model are resolving less and modelling more areas of the total process, and if the simulation accuracy is not largely affected, the feasibility of CFD simulation processes is considerably increased.

Bibliography

- Blanquart, G.;Pitsch, H. (2008). Large eddy simulation of a turbulent buoyant helium plume. *Center for Turbulence Research*, 245–251.
- Buresti, G. (2015). A note on stokes' hypothesis. *Acta Mechanica* 226(10), 3555–3559.
- Chai, X. and K. Mahesh (2012). Dynamic τ -equation model for large-eddy simulation of compressible flows. *Journal of Fluid Mechanics* 699, 385–413.
- Chung, W. (2007). *A CFD Investigation of Turbulent Buoyant Helium Plumes*. Thesis.
- Chung, W. and C. B. Devaud (2008). Buoyancy-corrected k - ϵ models and large eddy simulation applied to a large axisymmetric helium plume. *International Journal for Numerical Methods in Fluids* 58(1), 57–89.
- Dai, Z., L. K. Tseng, and G. M. Faeth (1995). Velocity statistics of round, fully developed, buoyant turbulent plumes. *Journal of Heat Transfer* 117(1), 138–145.
- Davidson, L. (2017). *Fluid mechanics, turbulent flow and turbulence modeling*. Gothenburg, Sweden: Chalmers University of Technology.
- De Villiers, E. (2006). *The Potential of Large Eddy Simulation for the Modeling of Wall Bounded Flows*. Thesis.
- Fiates, J., R. R. C. Santos, F. F. Neto, A. Z. Francesconi, V. Simoes, and S. S. V. Vianna (2016). An alternative cfd tool for gas dispersion modelling of heavy gas. *Journal of Loss Prevention in the Process Industries*.

- Frei, W. (2013). <https://www.comsol.com/blogs/which-turbulence-model-should-choose-cfd-application/>.
- Gant, S. E. and A. Kelsey (2012). Accounting for the effect of concentration fluctuations on toxic load for gaseous releases of carbon dioxide. *Journal of Loss Prevention in the Process Industries* 25(1), 52–59.
- Gant, S. E., V. D. Narasimhamurthy, T. Skjold, D. Jamois, and C. Proust (2014). Evaluation of multi-phase atmospheric dispersion models for application to carbon capture and storage. *Journal of Loss Prevention in the Process Industries* 32, 286–298.
- Germano, M. (1999). *From RANS to DNS: Towards a Bridging Model*, pp. 225–236. Dordrecht: Springer Netherlands.
- Germano, M; Piomelli, U. M. P. C. W. H. (1991). A dynamic subgrid-scale eddy viscosity model. *Physics of Fluids* 3.
- Hansen, O. R., F. Gavelli, M. Ichard, and S. G. Davis (2010). Validation of flacs against experimental data sets from the model evaluation database for lng vapor dispersion. *Journal of Loss Prevention in the Process Industries* 23(6), 857–877.
- Huang, S. and Q. S. Li (2010). A new dynamic one-equation subgrid-scale model for large eddy simulations. *International Journal for Numerical Methods in Engineering* 81(7), 835–865.
- Kim, W.-W. and S. Menon (1995). *A new dynamic one-equation subgrid-scale model for large eddy simulations*. Aerospace Sciences Meetings. American Institute of Aeronautics and Astronautics.
- Kumar, R. and A. Dewan (2014). Urans computations with buoyancy corrected turbulence models for turbulent thermal plume. *International Journal of Heat and Mass Transfer* 72, 680–689.
- Lindroth, D. (2013). *Large Eddy Simulation of Flow and Heat Transfer in a Pipe with Corrugated Walls*. Thesis.

- OpenFOAM (2013). <https://openfoam.org/release/2-2-0/documentation-function-objects/>.
- OpenFOAM (2017). <http://www.openfoam.com/>.
- Pham, M. V.; Plourde, F. D. K. S. (2007). Direct and large-eddy simulations of a pure thermal plume. *Physics of Fluids*.
- Pham, L. H. H. P. and R. Rusli (2016). A review of experimental and modelling methods for accidental release behaviour of high-pressurised co2 pipelines at atmospheric environment. *Process Safety and Environmental Protection 104, Part A*, 48–84.
- Pruett, C. D.; Gatski, T. B. G. C. E. T. W. D. (2003). The temporally filtered navier-stokes equations: Properties of the residual stress. *Physics of Fluids 15(8)*, 2127–2140.
- Rian, K. E., B. Grimsmo, B. Lakså, B. E. Vembe, N. I. Lilleheie, E. Brox, and T. Evanger (2014). Advanced co2 dispersion simulation technology for improved ccs safety. *Energy Procedia 63*, 2596–2609.
- Schleder, A. M. and M. R. Martins (2016). Experimental data and cfd performance for co2 cloud dispersion analysis. *Journal of Loss Prevention in the Process Industries 43*, 688–699.
- Shabbir, A. and W. K. George (1994). Experiments on a round turbulent buoyant plume. *Journal of Fluid Mechanics 275*, 1–32.
- Tieszen, S. R.; Domino, S. P. B. A. R. (2005). Validation of a simple turbulence model suitable for closure of temporally-filtered navier stokes equations using a helium plume. Report, Sandia National Laboratories.
- Versteeg, H.; Malalasekera, W. (2007). *An Introduction to Computational Fluid Dynamics: The Finite Volume Method* (Second ed.). Pearson Education Limited.
- Windfinder (2017). <https://www.windfinder.com/wind/windspeed.htm>.
- Woolley, R. M., M. Fairweather, C. J. Wareing, C. Proust, J. Hebrard, D. Jamois, V. D. Narasimhamurthy, I. E. Storvik, T. Skjold, S. A. E. G. Falle, S. Brown, H. Mahgerefteh,

- S. Martynov, S. E. Gant, D. M. Tsangaris, I. G. Economou, G. C. Boulougouris, and N. I. Diamantonis (2014). An integrated, multi-scale modelling approach for the simulation of multiphase dispersion from accidental co2 pipeline releases in realistic terrain. *International Journal of Greenhouse Gas Control* 27, 221–238.
- Worthy, J. (2003). *Large Eddy Simulation of Buoyant Plumes*. Phd thesis.
- Zhiyin, Y. (2015). Large-eddy simulation: Past, present and the future. *Chinese Journal of Aeronautics* 28(1), 11–24.
- Zhou, X., K. H. Luo, and J. J. R. Williams (2001). Large-eddy simulation of a turbulent forced plume. *European Journal of Mechanics - B/Fluids* 20(2), 233–254.